Consequences of introducing a cut-out wave height on a floating wind turbine concept

Jonas Skaare Amundsen

Norwegian University of Life Sciences
Department of Mathematical sciences and technology
Master Thesis 30 Credits 2013

This page is left blank intentionally.

Preface

This master's thesis marks the end of a five year Master of Science in Environmental Physics and Renewable Energy at The University of Life Sciences (UMB) in Ås. During the years at UMB, my interest and knowledge for renewable energy has grown and it was therefore a great privilege to be able to write a thesis within offshore wind power, on the floating turbine concept TLB. It has been motivating to work on such a concrete project, where several students are looking at different aspects of the concept; hopefully, my thesis can be a useful contribution in the research of the TLB.

Since my background is energy physics and not mechanics, I have focused on the aspects regarding energy production and the negative consequences of introducing the cut-out wave height, namely energy loss. The data processing through programming in MATLAB has sometimes been difficult and frustrating, but I feel that I have learned a lot these four past months. In order to compare the energy loss with a gain in load reduction, load simulations on the TLB has been performed by Ph.D Anders Myhr. He has been helpful through the entire thesis process and increased my understanding for the mechanical properties of the turbine.

Help has also been provided by the Norwegian Meteorological Institute regarding meteorological measurements and wave forecasting by Knut Iden, Reidun Gangstø, Birgitte Furevik and Yvonne Gusdal. Kenneth Johannessen Eik at Statoil has provided useful information about extreme wave prediction, while Erik Berge and Knut Harstveit from Kjeller Vindteknikk gave useful input to the thesis in a meeting in April. Associate professor Petter Heyerdahl has in general been a great inspiration to me through subjects and other lectures at UMB and I would also like to thank my fellow students and friends for useful input to the thesis, besides making my years at Ås unforgettable.

Finally, I wish to thank my supervisor Tor Anders Nygaard for giving me an interesting problem to work with. He has contributed greatly to the thesis work by giving very concrete guidance and through his natural positivity. This has motivated me to do my best when working with and writing this thesis.

Jonas Skaare Amundsen,
Ås, 14th of May 2013

Abstract

This master's thesis has investigated the consequences of implementing a survival mode system on the floating wind turbine concept Tension-Leg-Buoy (TLB) which shuts down the turbine at the cut-out wave height $H_{s,cut\text{-}out}$. The purpose of this is to reduce loads on the turbine structure at extreme wave conditions. One possible system is to move the top mooring lines upwards to the root of the nacelle, which has the potential of reducing loads in both mooring lines and anchors. If this is achieved, the excess buoyancy can be reduced by making the floater smaller which again reduces the material cost of the turbine.

The downside of such a system is that the some of the annual energy production from the wind turbine or wind farm will be lost since the turbine does not produce power in survival mode. This leads to a yearly income loss which in total must be lower than the cost reduction obtained from using less materials in the turbine components, in order for the system to reduce the total cost of energy delivered by the turbine.

By using time series of meteorological data sets containing wind speed and significant wave height from measurement stations in the North and Norwegian Sea, the energy loss at different values of $H_{s,cut\text{-}out}$ for all the sites has been found. If an energy loss of below 1% is accepted, the optimal cut-out wave height for the various sites obtains a value of between 8 and 9 metres (significant wave height). Scaling of the wave data has shown that $H_{s,cut\text{-}out}$ could be lower for milder wave climates. Additionally, three different control strategies for the survival mode system have been developed. The simulations using these strategies indicate that a strategy combining measurements and wave forecasts has the best overall performance, but these results rely on relatively high accuracy in the forecasting of wave heights.

Load simulations on the TLB have shown that there are still many challenges left to solve with the survival mode system using reconfiguration of mooring lines. There was no clear trend that the system is capable of reducing overall loads, which prevents any reduction in the mass of the floater. Nevertheless, the findings regarding energy loss and control strategies, which has the been the main focus of this thesis, will anyhow be valid for any survival mode system. These results may be used further even though the current concept does not achieve the load reductions required to bring down the material cost of the turbine.

Sammendrag

Denne masteroppgaven har undersøkt konsekvensene av å implementere et overlevelsessystem for det flytende vindturbinkonseptet Tension-Leg-Buoy som slår av turbinen ved en *cut-out* bølgehøyde $H_{s,cut\text{-}out}$. Hensikten med dette er å redusere belastninger på turbinen ved ekstreme bølgeforhold. Et mulig system er å flytte de øvre forankringslinene oppover mot nacellen, noe som kan bidra til å redusere belastninger i både forankringsliner og ankere. Hvis dette blir oppnådd, kan overskuddsoppdriften reduseres ved å gjøre flyteren mindre, noe som igjen minsker materialkostnaden til turbinen

Ulempen med et slikt system er at en del av den årlige energiproduksjonen fra vindturbinen eller vindparken tapes siden turbinen ikke leverer effekt når den er i overlevelsesmodus. Dette fører til et årlig inntekststap som total bør være mindre enn kostnadsreduksjonen som oppnås ved å bruke mindre materialer i turbinens komponenter, i hvert fall hvis systemet skal redusere den totale kostnaden til energien som leveres av turbinen.

Ved bruk av tidsserier med meteorologiske data (vindhastighet og signifikant bølgehøyde) fra målestasjoner i Nordsjøen og Norskehavet, har energitapet ved ulike verdier av $H_{s,cut\text{-}out}$ blitt regnet ut for hvert sted. Hvis man tillater at 1% av energien tapes, vil den optimale cut-out bølgehøyden for de ulike stedene ligge mellom 8 og 9 meter (signifikant bølgehøyde). Skalering av bølgedata har vist at $H_{s,cut\text{-}out}$ bør kunne være lavere for steder med mildere bølgeforhold. I tillegg har tre ulike kontrollstrategier for overlevelsessystemet blitt utviklet. Simuleringer har vist at en strategi som kombinerer målinger med bølgevarsler fungerer best, men dette vil avhenge av en relativt høy nøyaktighet på værvarslinga.

Lastsimuleringer på TLB'en har vist at det fortsatt er mange utfordringer å løse med et overlevelsessystem som benytter rekonfigurasjon av forankringsliner. Det var ingen klar tendens at systemet var i stand til å redusere laster, noe som forhindrer en massereduksjon i flyteren. Likevel vil resultatene som omhandler energitap og kontrollstrategier, som har vært hovedfokuset i denne oppgaven, gjelde for et hvilket som helst overlevelsessystem. Resultatene kan derfor benyttes videre selv om det nåværende overlevelsessystemet ikke oppnår de nødvendige lastreduksjonene som trengs for å få ned materialkostnaden på turbinen.

Table of Contents

List of Figures

List of Tables

Nomenclature

Wind power

Symbol	Explanation	Unit
α	Shear exponent	-
β	Pitch angle	$^\circ$
λ	Tip speed ratio	-
ρ	Air density	kg/m^3
$p(v)$	Probability of wind speed	-
u	Mean wind speed	m/s
$u_{anemometer}$	Mean wind speed measured at anemometer	m/s
$u_{10\,m}$	Mean wind speed 10 metres above ground	m/s
u_{hub}	Mean wind speed in hub height	m/s
$u_{cut-out}$	Cut-out wind speed	m/s
v	Horizontal wind speed	m/s
$v(z)$	Horizontal wind speed at height z	m/s
$v(zref)$	Horizontal wind speed at reference height	m/s
ω	Rotor angular velocity	rad/s
z	Height above ground	m
A	Rotor area	m^2
AEP	Annual energy production	GWh
C_p	Power coefficient	-
$C_{O\&M}$	Cost of operation and maintenance	€
C_c	Capital cost	€
CoE	Cost of energy	€/MWh
E	Energy output	kWh
F	Force	N
FCR	Fixed count rate	%
P	Power output	kW
P_{rated}	Rated power output	kW
T	Rotor torque	Nm
Z_{hub}	Hub height	m
$Z_{anemometer}$	Anemometer height	m

Waves

Term	Symbol	Unit
α	Weibull scale parameter	m
β	Weibull shape parameter	-
a	Wave amplitude	m
c_g	Wave group velocity	m/s
c	Rate of propagation	m/s
d	Ocean depth	m
ϵ	Gumbel scale parameter	m
f	Wave frequency	Hz
ϕ	Phase angle	rad
f_p	Peak frequency	Hz
g	Gravitational acceleration	m/s^2
k	Wave number	m^{-1}
λ	Wave length	m
m_0	Total variance of wave spectrum	m^2
η_0	Mean elevation	m
ρ_w	Density of water	kg/m^3
σ_{H_s}	Standard deviation of significant wave height	m
t	Time	s
θ	Gumbel shape parameter	-
ω	Angular wave frequency	s^{-1}
$BIAS$	Wave forecast bias	m
E	Wave energy	J/m^2
H_z	Zero-crossing wave height	m
H_s, $H_{1/3}$, H_{m0}	Significant wave height	m
H_{max}	Maximum wave height within a measurement period	m
$H_{s,50}$	50 year extreme significant wave height	m
$H_{s,cut-out}$	Cut-out wave height	m
$H_{s,re\ cut-in}$	Re cut-in wave height	m
$H_{s,measurement}$	Significant wave height measurement	m
$H_{s,forecast}$	Significant wave height forecast	m
$H_{s,mean}, \bar{H}_s$	Mean significant wave height	m
$N_{reconfig}$	Number of yearly reconfigurations	-
$RMSE$	Root mean square error	m
T	Wave period	s
T_z	Zero-crossing wave period	s
T_p	Peak period	s
T_r	Return period	year

Abbreviations

Abbreviation	Meaning
DNMI	The Norwegian Meteorological Institute
ECMWF	European Centre for Medium-Range Weather Forecasts
FAR	False alarm ratio
FFT	Fast Fourier Transform
GEV	Generalized Extreme Value (distribution)
GP	Generalized Pareto (distribution)
IEC	International Electrotechnical Committee
IFE	Institute for Energy Technology, Norway
JONSWAP	Joint North Sea Wave Project (spectra)
NREAP	National Renewable Energy Action Plan
NREL	National Renewable Energy Laboratory, USA
PDF	Probability density function
PM	Pierson-Moskowitz (spectra)
SWAN	Simulating Waves Nearshore
TLB	Tension-Leg-Buoy
TLP	Tension Leg Platform
WAM	Wave prediction Model
WMO	World Meteorological Organization

Chapter 1

Introduction

1.1 Background

Worldwide, there is a huge technical potential for electricity production from wind power and the industry has been steadily growing for the last decade at a rate of 25 - 30% annually[1, 2]. Today, most of the wind energy is produced by turbines located onshore, but this might change in the future due to the great advantages of offshore wind power. In many countries, the construction of onshore wind farms is limited by the visual impact on nature, environmental impact on bird life and the lack of inexpensive land. The transportation of large wind turbine components to the wind farm site can also be challenging in some cases[1].

Despite of these advantages, offshore wind power is not as developed yet due to a higher cost of energy and higher risk related to constructing and operating an offshore wind farm. Most of the offshore wind farms in the world are found in the North Sea, outside the coast of the United Kingdom, Denmark, Belgium, Germany and the Netherlands[2]. The construction of the wind farms has only been made possible by different support schemes, whose purpose is to kick-start the offshore wind industry so that cost reductions can be made, thus making offshore wind power more competitive. All offshore wind farms today are located in shallow waters (less than 50 metres), meaning the the turbines are bottom-fixed either with a monopile or jacket structure[2]. A few individual floating turbines are installed for research purposes, but large offshore floating wind farms are not mature enough to enter this market yet. Still, there is a great offshore wind resource potential in countries like USA, China and Japan where the deeper waters will require the use of floating wind turbines.[3]

Several floating turbine concepts exist as prototypes or on the drawing table, but none of them are at the moment commercial alternatives to bottom-fixed turbines. To achieve the necessary cost reduction to make a floating concept economically viable, there are several alternatives, such as:

1. Optimizing the design of the wind turbine
2. Developing a strategy for the wind turbine which reduces loads on the turbine structure

The first alternative is all about finding a floating concept that is both cheap and reliable at the same time. One example is to reduce the material cost related to the floater, the component which makes the turbine float. Still, this will make the turbine structure more vulnerable to damage from wind and wave forces; it is therefore important to find the right balance between these two factors.

An example of the second alternative is to shut down the wind turbine at high wind speeds (>25 m/s) to reduce wind loads, a common strategy for most large wind turbines both onshore and offshore. By reducing the most extreme loads (dimensioning loads) the turbine has to withstand, the material cost of the structure is minimized. The cut-out wind speed also has a positive effect on the long-term fatigue loads, which also are reduced. This prolongs the life time of the turbine and lowers the cost of maintenance and repairs. Since this is done without significantly reducing the yield (energy output) of the turbine, the total cost of energy is minimized. A similar shutdown strategy could also be designed to reduce wave loads at rough sea. This master's thesis investigates the effect of combining cost reduction alternative 1 and 2 on a floating wind turbine concept.

1.1.1 The TLB with cut-out wave height

The Tension-Leg-Buoy (TLB) is a floating wind turbine concept which has been further developed by professor Tor Anders Nygaard at IFE/UMB together with Ph.D and Master students through several years. The goal of the research is to develop a floating wind turbine that may be used in large offshore wind farms with several hundred turbines. The research is focused on minimizing costs by optimizing the design of the turbine, reducing loads on the structure and developing clever operation strategies for the wind turbine/farm.[4]

The current version of the TLB is called the TLB B and is described more in detail in section 2.6.2. The TLB B uses considerably less steel compared to the HyWind turbine installed outside the coast of Norway[5]. It is stabilized by six taut mooring lines attached at two different points on the turbine, see figure 2.7. The turbine structure is dimensioned to withstand a 100-year wave, which limits further mass reduction of the concept. However, this could be overcome by introducing an operation strategy where the turbine is shut down at high waves and the upper mooring lines are moved to the top of the turbine tower. When the reconfiguration of the mooring lines is complete the turbine is in "survival mode" and does not produce energy. When the sea calms down and the wave height is reduced, the mooring lines are moved back to their original position and the turbine resumes operation.

There are other ways a survival mode system could work, like for example ballasting the floater. As with the reconfiguration of the mooring lines or any other survival mode system, the point is to reduce extreme wave loads on the structure at high waves. For example, if the force amplitudes on the mooring lines and anchors at high waves are decreased, this allows for a smaller floater to be built in the TLB B, thus reducing the total material cost of the turbine. On the other hand, shutting down the turbine would lead to a certain loss in energy production and consequently a loss of income. This loss must be compensated by a reduction in loads and costs of the turbine structure; a so-called *trade-off*. To maximize the trade-off from introducing a survival mode system, one seeks to find the optimal cut-out wave height $H_{s,cut\text{-}out}$ where the gain from shutting down the turbine exceeds the loss of energy.

1.2 Goal of the thesis

The goal of this master's thesis is to investigate the effect of introducing a cut-out wave height for the floating wind turbine concept TLB B. The study uses coherent wind and wave data measured in the North Sea and Norwegian Sea over several years and a simulation tool for load calculations on the TLB B. By weighing the energy loss against the material cost reduction of the turbine, the thesis aims to find the optimal $H_{s,cut\text{-}out}$ and the optimized turbine structure which can be used in large floating wind farms.

1.2.1 Objectives

The objectives for the thesis are as follows:

1. To find the ideal energy loss at different cut-out wave heights with the assumption that the time spent to go into survival mode is negligible
2. To develop various control strategies for the reconfiguration system and calculating the real energy loss assuming different reconfiguration times
3. To calculate extreme loads on the turbine structure in operational and survival mode by using the in-house simulation tool 3Dfloat and finding an optimized floater with reduced material costs

By scaling the available wind and wave data to fit climates in other places in the world, one can examine the possibility of designing several versions of the TLB B; each adapted to the different markets for floating wind turbines with its own optimal $H_{s,cut\text{-}out}$.

1.2.2 Scope and limitations

The main purpose of this thesis to consider whether a survival mode system that operates at high waves is a good idea or not. Although there is much focus on finding the optimal cut-out wave height for the different sites, it must be mentioned that there are many uncertainties that could affect the choice of the correct $H_{s,cut\text{-}out}$. Some of these uncertainties are related to the energy production estimates calculated from the wind data, which have been performed using several assumptions, such as:

- The wind speed measurements have not been disturbed by nearby obstacles
- The 10-minute mean wind speed is constant between measurements (interval: 20 min)
- The shear exponent is constant
- The data set for each location is representative for a longer period of time ($\simeq$ 20 years)
- The wind turbine is not stopped for maintenance

In addition to this, one turbine is assumed to represent a large wind farm when it comes to the power production and the energy loss from introducing the cut-out wave height. In real life, many of the wind turbines would experience wake losses from upstream turbines, causing the average energy production of the turbines in a wind farm to be less than that of an individual, undisturbed turbine.

When it comes to the load analysis performed in 3Dfloat, only extreme loads are considered. It is possible that the reconfiguration system for the mooring lines or other survival mode systems could reduce the fatigue loads on the floating turbine, but neither a fatigue load analysis nor an economic analysis of the energy loss versus the material cost reduction has been performed.

The scaling of the data from the North Sea and Norwegian Sea to other locations on Earth is highly uncertain since the weather systems controlling the wind and waves on these places are very different. Therefore the Weibull parameters for wind speed and wave height distributions could differ substantially, making the scaling problematic. Nevertheless, a linear downscaling of wave data has been executed to qualitatively investigate the effect on the optimal $H_{s,cut\text{-}out}$. Still, the best (and scientific) way to do this would definitely be to use original data from the specific locations.

1.3 Outline of the thesis

The outline of this thesis is as follows:

Chapter 2 gives an introduction to offshore wind power and explains how electricity is produced from wind energy. It also gives an overview of different floating turbine concepts, including the turbine concept investigated in this master's thesis, the TLB B.

Chapter 3 will introduce important terminology within waves and wave analysis, explaining how ocean waves are measured and wave height data is analysed statistically. The chapter also gives some insight in extreme wave statistics and the accuracy of wave forecasting.

Chapter 4 will explain how wind and wave data has been collected and analysed together with the load analysis in 3Dfloat to investigate the objectives of the thesis.

Chapter 5 will give an overview of key results that has been found through the data analysis.

Chapter 6 discusses the method and the main findings.

Chapter 7 concludes the work and provides recommendations for further studies.

The readers of this master's thesis are assumed to have some knowledge within physics, statistics and wind power, but the theory chapters (2 and 3) should provide enough information for anyone to understand the approach and results of the thesis.

Chapter 2

Offshore wind power

2.1 Offshore wind power status

Offshore wind power has grown significantly the last few years, with a total global installed capacity of 5.5 GW at the end of 2012. 4995 MW of this is located in European Union (mostly in the North Sea) and produce enough energy to cover 0.5% of EU's total electricity consumption of 3349 TWh. In comparison the onshore installed capacity in the EU is 101 GW, covering 6.4% of EU's electricity consumption. Still, more and more offshore wind farms are likely to be constructed towards 2020 according to the National Renewable Energy Action Plan (NREAP) which was delivered by all EU countries as a tool to reach the 2020-targets. Offshore wind power also have advantages compared to onshore (e.g. higher wind speeds) and do not face the same challenges as lack of land and high public resistance[1]. In combination with technology development and cost reduction, offshore wind power can grow to be play an important role in the European electrical market already before 2020.[2]

The UK is by far the largest offshore wind country in the world (2948 MW), followed by Denmark (921 MW) and China (509.5 MW)[2]. Towards 2020 Germany, Belgium, Netherlands and France have ambitious plans for offshore wind farms, but it is uncertain how much of the plans which will be realized. This depends especially on the size and stability of the support scheme for offshore wind power, since electricity prices in Europe are not high enough to cover the cost of the wind farm alone. The support scheme in the UK, the ROC, is probably the main reason that the country is in the leading position when it comes to developing offshore wind power in the world[6]. This has led to the construction of several large offshore wind farms, like Sheringham Shoal (317 MW), which is owned by the Norwegian companies Statkraft and Statoil[7].

2.1.1 Status of floating wind turbines

The offshore wind turbines installed in Europe today are almost all bottom-fixed at depths of around 10-40 metres. In fact, there are only four floating turbines installed in European waters, of which only two are full scale grid-connected turbines. Still, in the United States, China, Japan and several places in Europe, there is a great offshore wind potential in water deeper than 30 metres. Even though bottom-fixed turbines might be installed in depths greater than 50 metres, there comes a limit where floating turbines are cheaper to construct, install and maintain. To be able to utilize the areas with offshore wind potential one has to develop floating technologies.[2]

One example is HyWind, a 2.3 MW floating turbine developed by StatoilHydro and Siemens using a Spar-buoy concept, see section 2.6. It was installed outside Karmøy on the west coast of Norway in 2009 and has been operating ever since surviving rough weather conditions[8]. The next step for HyWind is a demonstration project which will consist of four turbines deployed outside the coast of Maine, USA[9]. Several prototypes using different floating technologies are in development and will be constructed the next few years. The final goal is to construct large offshore floating wind farms with the same size as current bottom-fixed wind farms($\simeq$ 100 turbines). It is not known how long it will take before floating wind turbines reach this level of maturity, but somewhere around year 2020 could be a good guess[8].

2.2 The wind turbine

The purpose of any wind turbine is to convert wind energy into electrical energy. The most common large scale wind turbine used for offshore wind farms is an upwind three bladed horizontal axis turbine with a rated power of several megawatts. The most used turbine in European offshore wind farms is the Siemens 3.6 MW turbine, but future wind farms are likely to use wind turbines with rated power above 5 MW.[2]

2.2.1 Components of the wind turbine

A wind turbine consist of the following main components[10]:

- Rotor blades
- Nacelle
- Tower
- Foundation (onshore or bottom-fixed)
- Floater (floating)
- Stationkeeping system (floating)

An example of a floating wind turbine concept, the Tension Leg Buoy (TLB), is shown in figure 2.1. Although the relative dimensions of the components are not shown, the figure demonstrates that the tower must be tall enough to avoid that the rotor blades come in contact with water. For a 5 MW turbine the typical height for the turbine tower is around 90-100 metres, while the diameter of the rotor is between 100-120 metres.[11, 5]

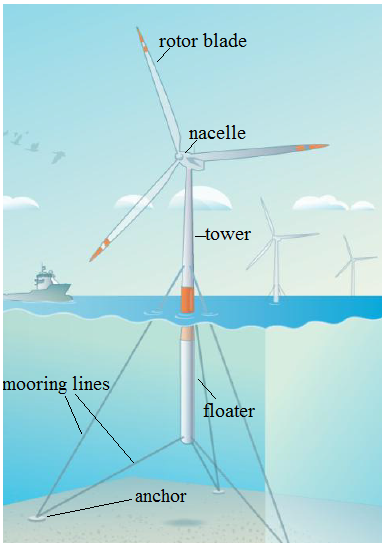

Figure 2.1: *Components for the TLB floating wind turbine concept*[4]

2.2.2 Power curve

A wind turbine converts wind power to shaft power through the rotor blades which is converted to electrical power through the generator. The power produced by a horizontal axis wind turbine with pitch regulation is written as[12]:

$$P = \frac{1}{2}\rho A v^3 C_p(\lambda, \beta) = \omega T \tag{2.1}$$

where ρ is the density of air ($\simeq 1.225$ kg/m^3), A is the rotor area, v is the horizontal wind speed in the rotor area, C_p is the power coefficient, ω is the angular velocity of the rotor and T is the rotor torque. λ describes the relationship between the tip speed of the rotor and the wind speed, while β is the pitch angle of the rotor blades.

The power curve for a wind turbine shows the power produced by the generator for a given wind speed. The assumption that the wind speed in the rotor area is homogeneous is not correct due to wind shear and turbulence. Still, for energy production calculations using 10-minute mean wind speed one can assume that the average wind speed in the rotor area is equivalent to the wind speed measured at hub height[13]. The power curve for three different wind turbines is shown in figure 2.2:

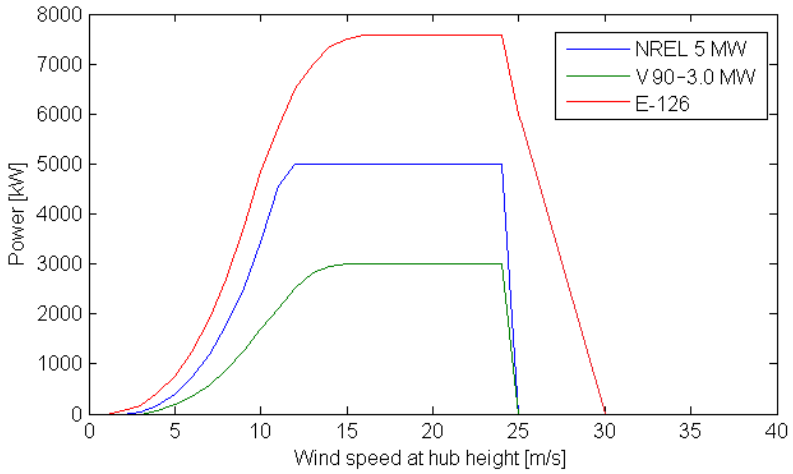

Figure 2.2: *Power curves for Enercon's E-126 7.5 MW[14], Vestas' V90-3MW[15] and NREL's 5 MW [11] turbine*

As it can be seen from the figure, the wind turbine starts to produce power around 2 - 4 m/s, which is called the cut-in wind speed. Then the power increases with v^3 until the wind speed reaches the rated wind speed (around 12 - 15 m/s). When the turbine has reached rated power, the rotor blades start turning out of the wind. This is called pitching and makes the wind turbine stay at a constant power even though the wind speed increases. When the wind speed reaches 25 m/s (cut-out speed) the turbine cease power production by pitching the blades completely (90 degrees) and shut down. This is done to prevent fatigue loading on the turbine structure. Although this leads to a loss in energy production, this is considered less

important since wind speeds are rarely above 25 m/s (at least onshore). There are different control systems for how the turbine restarts after shutdown. One is that the turbine restarts when the wind speed (2 or 10 minute mean) drops below cut-out speed, which is called dead band controlled[16]. Another is that the turbine cuts in when the mean wind speed drops below a re cut-in speed (e.g 20 m/s), a control strategy known as high-wind hysteresis.

Enercon turbines, like the E-126, uses a special patent called storm control which prevents a complete shutdown at 25 m/s.*"This is achieved by slightly pitching the rotor blades out of the wind. Once the wind speed drops, the blades turn back into the wind and the turbine immediately resumes operation at full power. This prevents yield-reducing shutdown and start-up procedures"*[17]. It should be mentioned that Enercon has not entered the offshore wind turbine market at the moment. Still, other wind turbine manufacturers for offshore wind power, like Siemens, is looking into this kind of system to increase power production due to the higher wind speeds offshore. Siemens calls their solution the High Wind Ride Through application[18].

2.3 Wind speed variation with height

Due to friction with the ground or the ocean surface, the wind speed will increase with height. This is known as wind shear, see figure 2.3. The wind shear in a place depends on factors like the roughness of the ground and shape of the terrain. The shear also depends on the atmospheric stability, which varies in time. The vertical wind profile can be described more in detail using a logarithmic profile, but for simple engineering applications, it is more convenient to use the power law profile which only depends on an empirical shear exponent α and is given by[13]:

$$V(z) = V_{zref}\left(\frac{z}{z_{ref}}\right)^{\alpha}, \tag{2.2}$$

where V_{zref} is the mean wind speed in the reference height z_{ref} (e.g measurement height) and $V(z)$ is the mean wind speed at height z. α determines the shape of the wind profile; a high value ($\alpha \simeq 0.20$) indicates rough terrain, while a low value ($\alpha \simeq 0.10$) indicates very flat terrain or ocean, see figure 2.4[13].

The uncertainty in the use of the power law can be high because the shear exponent can vary significantly in time and is not necessarily valid for all heights. Extrapolating wind speed measurements at 10 metres altitude up to hub height can in the worst case lead to 40% errors in energy production calculations. The error can be reduced by applying a correction factor to the power law which includes temperature, direction, pressure and even waves for offshore sites, but these models soon get very complicated[19]. The easiest thing is there to have the measurement height as close to the hub height as possible, making the use of the power law profile more reliable.

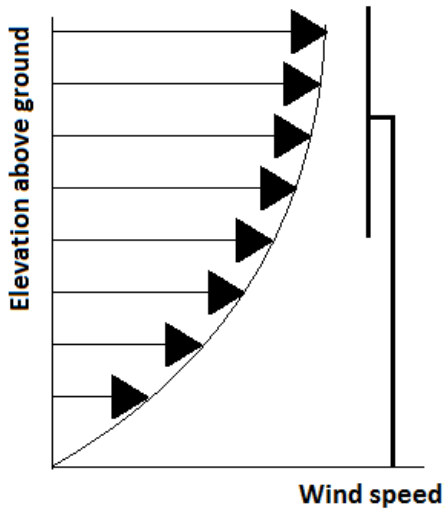

Figure 2.3: *Wind shear in front of a wind turbine*

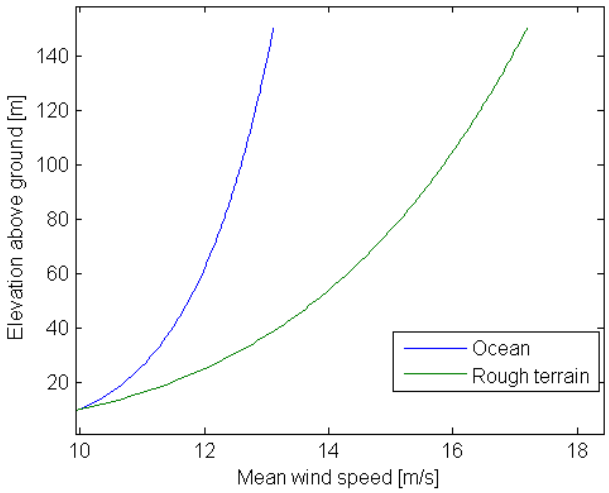

Figure 2.4: *Wind shear in different terrain*

2.4 Wind variation and power production

While most wave types are caused by the wind, the wind is driven by the pressure difference between two places. Due to the low density of air compared to the relative high density of water, the wind speed changes rapidly compared to waves. This is known as turbulence and is quantified by the turbulence intensity, which describes the variation of the wind speed around the 10-minute mean wind speed. The turbulence intensity can have a value of between 10 - 40% depending on the location[13]. Places with higher wind speeds and flat terrain (e.g offshore sites) have lower turbulence intensity. This is an advantage since high turbulence will cause more fluctuating loads on the turbine structure that can lead to fatigue in the long-term[20]. A high turbulence intensity might also lead to problems for the power quality known as flicker[21].

Although short-term variation of wind speed can contribute to some error in the calculation of the annual energy production (AEP) from a wind turbine[19], the 10-minute wind speed is usually considered sufficient for estimating the AEP. The energy production for a wind turbine considering that the turbine is not stopped for maintenance is given as:

$$AEP = \sum_{i=1}^{N} P_i(v) \cdot t_i \tag{2.3}$$

where N is number of measurements in a year, t_i is the time interval (usually 10 minutes) and $P_i(v)$ is the power of the turbine which is calculated by inserting the wind speed v into the power curve of the given turbine. Normally the AEP is given in kWh (or MWh,GWh etc.), meaning that $P_i(v)$ is given in kW and t_i in hours. It is also possible to fit the wind speed data for a year to a Weibull distribution (just as for waves in figure 3.10) and calculate the power production for different wind speeds using:

$$E(v) = p(v) \cdot P(v) \tag{2.4}$$

where $p(v)$ is the probability of a certain wind speed. The AEP can then be calculated by summing $E(v)$ for all wind speeds.

An important parameter for all electricity production utilities is the capacity factor, which is defined as the ratio between the AEP and the energy that would have been produced if the utility had been running on full capacity all year (8760 h):

$$\text{Capacity factor} = \frac{\text{AEP}}{P_{rated} \cdot 8760 \text{ h}} \tag{2.5}$$

Another way to measure the power production is using the full load hours[13]:

$$\text{Full load hours} = \frac{\text{AEP}}{P_{rated}} \tag{2.6}$$

The capacity factor is considerably higher for offshore sites (3500 - 4000 full load hours) due to higher wind speeds compared to onshore sites, which on average has about 2000 full load hours. This means that a 5 MW turbine that produces about 10 GWh on an onshore site would produce roughly 17.5 - 20 GWh on an offshore site. Individual wind farms far-offshore are likely to reach up to 5000 full load hours in the future.[2]

2.5 Loads on offshore wind turbines

Any wind turbine placed offshore will have to endure forces from wind and waves. The forces affect different parts of the turbine and are known as structural loads. These loads cause stresses, deformation or acceleration of the structure and if a load exceeds the limit of parts or the whole structure, structural failure occurs. For an offshore wind turbine these might be cracks in the tower, damages to the rotor blade or mooring lines snapping. How a given turbine responds to wind and wave loads depends on the design of the structure and there can be large differences in response between bottom-fixed turbines and various floating technologies.[3]

There are two different loading situations that might cause structural failure in a wind turbine. The first is the ultimate/extreme failure situation where heavy wind and high waves single-handedly can cause structural damage. Every part of the structure must withstand the most extreme load expected in the life time of the wind turbine/farm, multiplied with a safety factor of 1.5 - 2.0[10]. The second situation is the deterioration of metal due to constant exposure of wind and waves that might lead to an ultimate failure in the long run, known as fatigue load. Fatigue must be controlled by inspection so that failure is avoided by maintenance and repair when necessary.[22]

The combined loading from wind and waves must be tested in models and experiments before a turbine is released on the market. In the model tests the turbine is run through different load cases which are defined in various standards, for example those made by the American Bureau of Shipping[10] or DNV[23]. By exerting the turbine to various wave and wind loads both in operational mode and shutdown, extreme and fatigue loads are calculated. An

example of a model test showing maximum load as a function of wind speed and significant wave height on a bottom-fixed turbine is shown in figure 2.5.

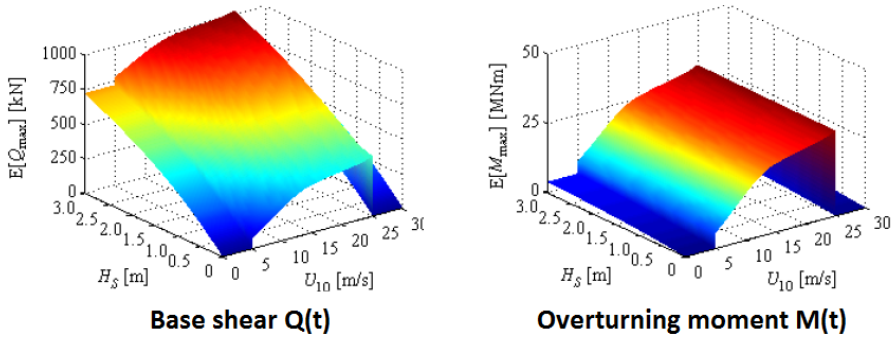

Figure 2.5: *The load response for a bottom-fixed turbine as a function of 10-minute mean wind speed u and significant wave height H_s.* [24]

As it can be seen on the figure, both the base shear and the overturning moment increases steadily with the wind speed until it stabilizes at rated power and is heavily reduced when the turbine shuts down at 25 m/s. For waves there are bigger differences; the base shear (forces acting on the tower at seabed level) increases with the significant wave height H_s (for definition, see section 3.2.3), but the overturning moment is almost insensitive to wave height[24, 25]. For floating turbines there are also parts that are minimally affected by the wave height, such as the rotor blades and the low-speed-shaft. Loads on the tower, floater and the mooring lines will on the other hand be greatly influenced by the design of the floating design.[3]

2.6 Floating wind turbine technologies

2.6.1 Main concepts

As mentioned in section 2.1.1, floating wind turbines will at some depth ($\simeq$ 50 metres) become more economically viable than bottom-fixed structures. Different floating technologies are often categorized by the design of the floater and the stationkeeping system. The designs are inspired by oil platforms, which differ in how they achieve stability in the pitch and roll movement. The most common floating concepts for wind turbines are the spar buoy, the tension leg platform (TLP) and the barge, see figure 2.6. It is also possible with a hybrid combining the three stability methods (e.g semi-submersible).[3]

The spar-buoy, which is the concept used for HyWind, becomes stable by using ballast to lower the centre of gravity. The TLP has excess buoyancy pushing it up, but is kept down by taut mooring lines which prevents heave (up and down) movement. The barge is stabilised by a large waterplane area and is moored by catenary lines. There are advantages and disadvantages with all the floating concepts, both with regards to material cost and loads [3, 8]. Which of the technologies that will take the leading role in floating offshore wind power in the future relies on the total cost of energy delivered by the wind turbine, see section 2.7.

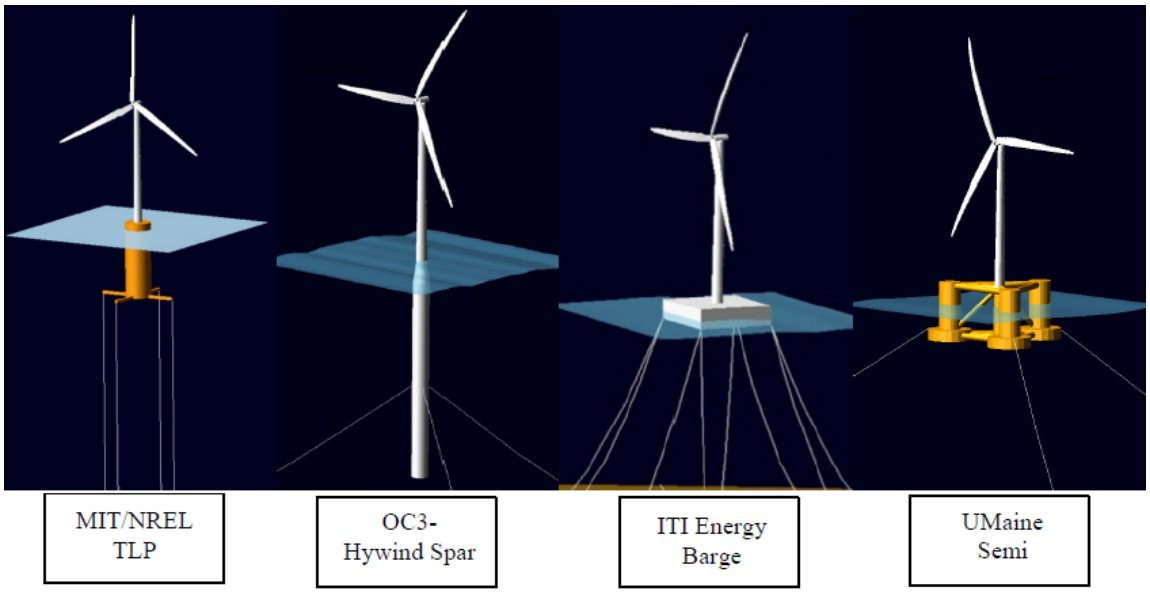

Figure 2.6: *Different floating turbine technologies*[3]

2.6.2 The Tension-Leg Buoy (TLB) floating wind turbine concept

The Tension-Leg Buoy or Taut-Leg-Buoy (TLB) was developed by researchers at MIT and NREL in 2005[1]. The TLB uses taut mooring lines attached on the bottom of the floater to the sea bed with gravity anchors. The difference from the TLP is that the mooring lines are inclined relative to the sea floor[1]. The TLB controls all linear and rotational movement of the turbine, which is kept still relative to the sea bed, and the turbine is actually more bottom-fixed than floating. The TLB has a great potential for reducing material costs and loads on the turbine structure, but will experience higher loads on mooring lines and anchors[4].

The TLB has been further developed by professor Tor Anders Nygaard at IFE/UMB together with Ph.D's Anders Myhr and Karl Jacob Maus, along with several master students. The work has consisted in developing and using a numerical tool for predicting dynamic response on offshore wind turbines called 3Dfloat. In addition, several wave tank tests have been executed both in Norway and France to compare computations with actual experiments. Through the research several concepts have been considered with the main goal of reducing loads and cutting costs by making the floater smaller[5]. The TLB has 2×3 mooring lines, the first pair placed on the bottom of the floater and the second pair attached as high up on the turbine tower as possible without conflicting with the rotor blades.[4]

One of the predecessors of the TLB, Njord, would have a reconfiguration system for the mooring lines to reduce loading on the whole structure[26]. At severe weather conditions the turbine would go into "survival mode" where the upper mooring lines would be moved to the root of the nacelle and reduce extreme loads. The current concept of the research group is called the TLB B, which is a 5 MW turbine that is unstable until the mooring lines are installed. The total mass of the TLB B is only 950 tons, compared to about 8000 tons for the

HyWind concept[5]. One of the next steps is to integrate the reconfiguration system for the mooring lines from Njord or other survival mode systems in the TLB B and develop a control system for how it should operate. An illustration of the TLB B in operational (standard) and survival mode is shown in figure 2.7:

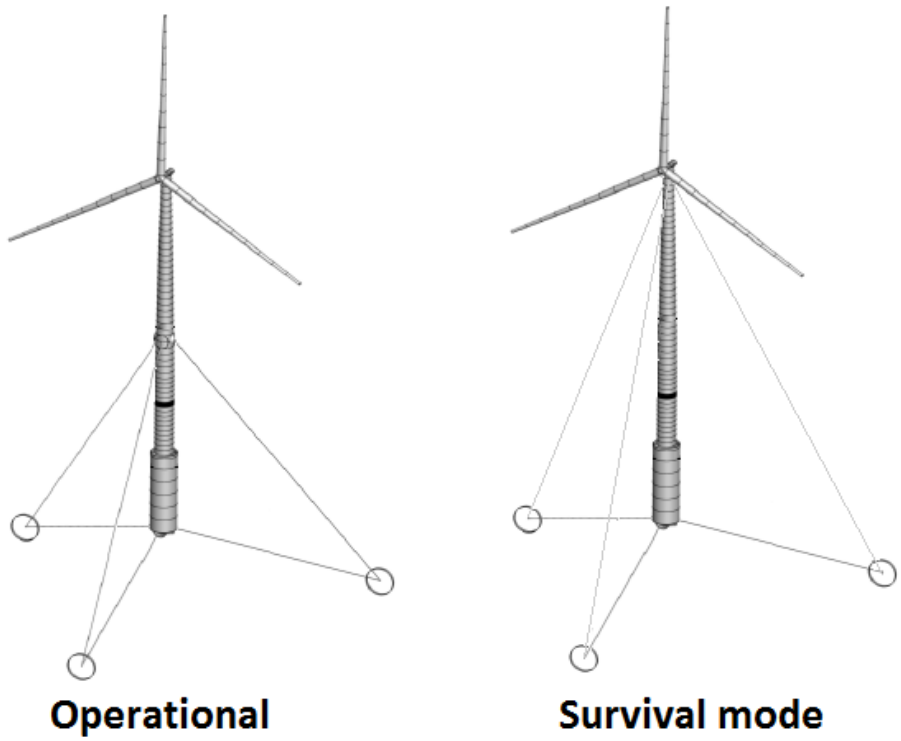

Figure 2.7: *The TLB B in standard and survival mode* [4]

2.7 Economy of offshore wind power

In order for any electrical energy production utility to become economically viable, the total income from electricity sale plus subsidies must be greater than the total life time cost of the utility. The cost of energy (CoE) is the unit cost to produce energy (in €/MWh) and is calculated by[13]:

$$CoE = \frac{C_c \cdot FCR + C_{O\&M}}{AEP}, \tag{2.7}$$

where $C_c \cdot FCR$ is the yearly capital cost discounted with the fixed charge rate and $C_{O\&M}$ is the average annual cost of operation and maintenance. For a wind farm, C_c is the cost of the wind turbines, electrical cables etc. and the cost of installing the wind farm, while $C_{O\&M}$ is dominated by maintenance costs because the fuel cost (i.e. wind) is free. The cost of energy can be minimized by increasing the energy production or by decreasing either the capital cost or maintenance cost; finding the right balance in equation 2.7 is therefore vital in order to make a wind farm project profitable.

Chapter 3

Waves and wave statistics

3.1 Basic definitions within wave analysis

In general, a wave (or a train of waves) is characterized by its period T, amplitude a, frequency f, length λ and rate of propagation c. These parameters are defined in figure 3.1 and relates to each other mathematically by:

$$c = \lambda f, \quad f = \frac{1}{T} \tag{3.1}$$

The top of the wave is called the crest and the bottom the trough. The total difference between these two is known as the wave height defined as $H = 2a$.

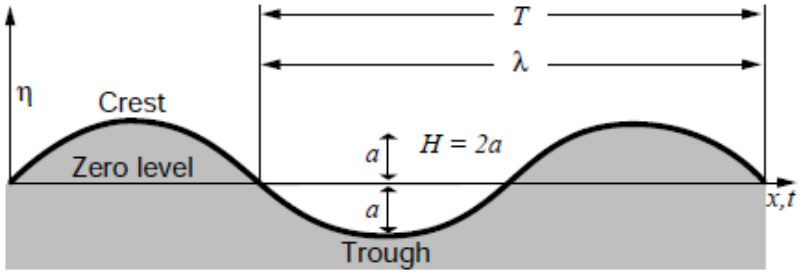

Figure 3.1: *Simple sinusoidal wave (Courtesy of WMO)*[27]

The wave profile η of this simple sinusoidal wave which repeats itself in time and space can be written[27]:

$$\eta(x,t) = a\sin(kx - \omega t), \tag{3.2}$$

where $k = \frac{2\pi}{\lambda}$ is the wave number and $\omega = \frac{2\pi}{T}$ is the angular frequency. For deep water waves, meaning that the depth d $> \frac{\lambda}{4}$, k and ω is related to each other by $\omega^2 = gk$, where g is gravitational acceleration. This gives another expression for the wave propagation c:

$$c = \frac{\lambda}{T} = \frac{\omega}{k} = \sqrt{\frac{g}{k}} \tag{3.3}$$

In deep water the wave length λ may be calculated from the following formula:

$$\lambda = \frac{gT^2}{2\pi} \tag{3.4}$$

In this thesis the spatial distribution of a wave field is not relevant since it is more interesting to understand the variation of wave height in one specific place; the placement of the wind

turbine. By setting $x = 0$ in equation 3.2 becomes the formula describing the motion of a wave buoy at a specific place:

$$\eta(t) = a \sin(-\omega t) \tag{3.5}$$

Another important property of wave is superposition. When waves collide with each other, the height of the resulting wave is determined by the mathematical sum of the individual waves. If the different parameters of two waves are equal (H, λ, T, direction, phase), the resulting wave will be twice as big as the individual waves. If the waves are 90 degrees out of phase, the waves will destruct each other completely and the resulting wave height will be zero. When two waves have different periods and/or heights the resulting wave profile will be less regular, see figure 3.2. At the ocean, the wave profile at a certain place is the sum of a number of simple waves, each with different wave heights, wave lengths, direction and periods. The simple waves are also in constant change due to changes in winds, meaning that the wave profile at a given place appears very irregular.

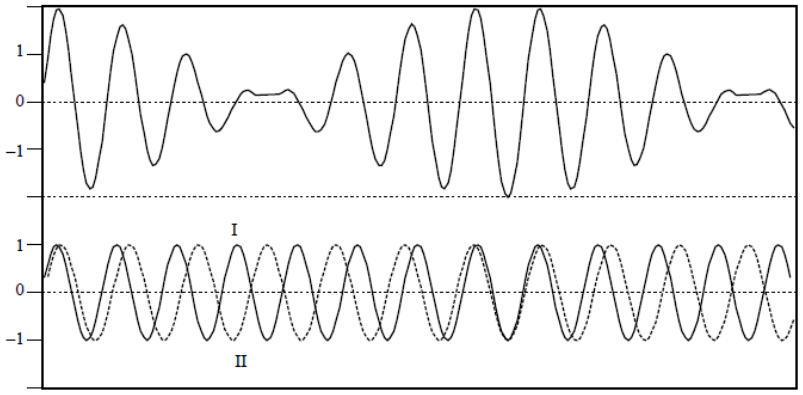

Figure 3.2: *Superposition of two simple waves with different properties (Courtesy of WMO)*[27]

Considering the elevation above a mean sea level at a given point of time as a sum of sinusoids with different properties is useful to understand which wave periods contains the most energy and will do most harm to offshore installations. This is done by Fourier analysis and is described in section 3.2.5.

Larger waves with similar properties tend to come in groups and although every wave has its own speed of propagation, it is useful to speak of a group velocity c_g. In deep water it is calculated by[27]:

$$c_g = \frac{c}{2}, \tag{3.6}$$

where c is calculated from equation 3.1 with the mean λ and T within the group. The wave group is the carrier of the wave energy and the wave group velocity also gives the velocity in which the wave energy is propagated. The wave energy (per unit area) has the expression[27]

$$E = \frac{1}{2}\rho_w g a^2 = \frac{1}{8}\rho_w g H^2 \tag{3.7}$$

where ρ_w is the density of water. When performing an Fourier analysis on a time series of wave heights, the spectrum obtained will show the wave energy at different frequencies/periods.

3.2 Short-term wave statistics

3.2.1 Measuring ocean waves

Waves on the ocean are created by different forces, such as wind, tides, gravity of the Earth and earthquakes. Waves caused by differences in atmospheric pressure(i.e. wind) are known as ordinary gravity waves and propagates horizontally on the ocean surface. Waves at sea can be divided into waves caused by local winds called wind sea, and waves coming in from other areas, namely swell[28]. While wind sea changes rapidly in wave height, period and direction, swell appear more like the sinusoids in which ocean waves are represented by.

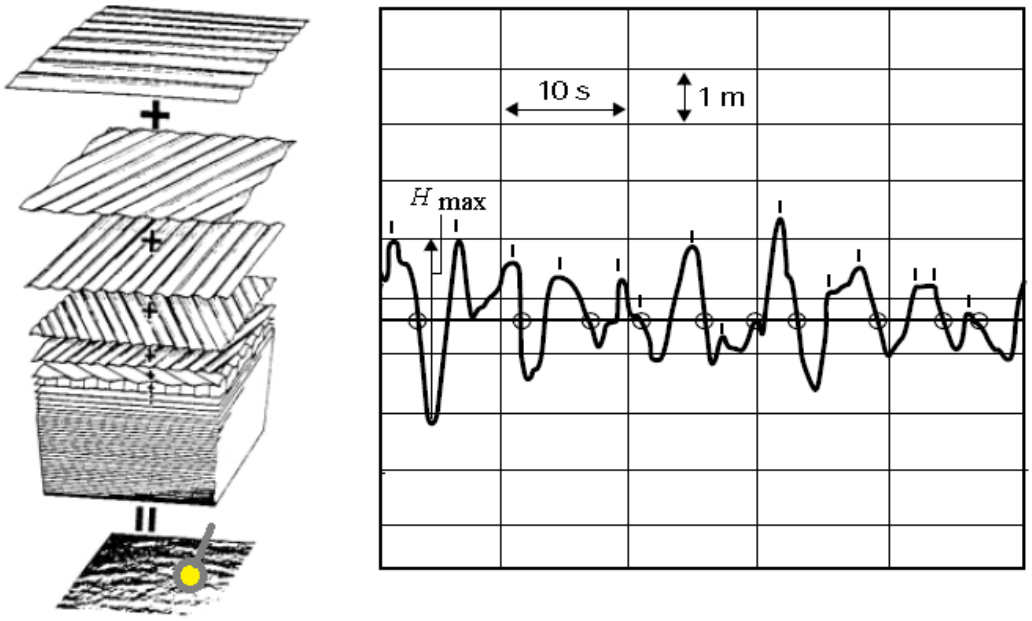

Figure 3.3: *Sample of a wave buoy record placed in irregular seas (Courtesy of WMO)*[27]

Ocean waves can be measured by wave buoys, which are placed at the desired point and measures wave height, period and direction several times a second. They are often placed with radio transmitters so data can be read live without having to sail out to collect them. Figure 3.3 shows the placement of a wave buoy (yellow dot) in the sea, which measures the elevation over the mean sea level over time. The irregular pattern measured consists of sums of regular wave fields propagating with different direction. An important aspect of the wave measuring is the zero down-crossings (or up-crossings) shown in the figure as circles, which indicates the time when the elevation crosses the mean sea level. The period T is the time distance between two down-crossings and the zero crossing wave height H_z is the vertical distance between the highest and lowest point within the period[27, 22].

The result of a wave buoy measurement is a time series of wave heights $(H_1, H_2, H_3...)$ with its period $(T_1, T_2, T_3...)$. As it can be seen on the figure, short-crested waves which do not cross the mean sea level are not registered as waves, at least not with its own height and period. For some applications, like Fourier analysis, raw time series of T and H_z with high temporal resolution is necessary. On the other hand, when looking at wave records for a longer time (days, weeks, months, years) it is necessary to process the measurements in order to avoid superfluous data. In the following sections, basic statistical methods for ocean waves are presented.

3.2.2 Short-term wave height distributions

Measurements of wave heights on a short-term basis tend to follow certain statistical distributions, like the Rayleigh distribution [25, 29]. If the time series in figure 3.3 had lasted for some hours, about 1000 waves would have hit the buoy. If one makes a histogram of the wave heights in the time series and make a smooth line, figure 3.4 is obtained. If the y-axis says *Probability* instead of *Number of waves*, the graph would show the probability density function (PDF) of the wave height time series, where the integral under the curve would be unity.

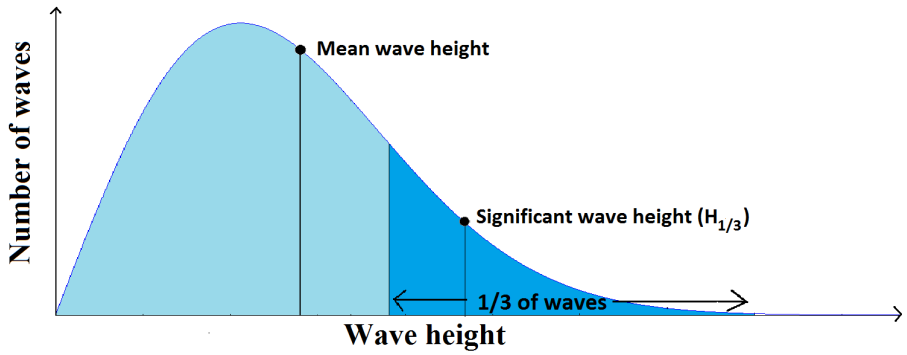

Figure 3.4: *Typical distribution of measured wave heights within a certain measurement time*

3.2.3 Significant wave height

Although a sea state could be described through the mean wave height, the *signficant wave height* H_s is used instead. The definition of the significant wave height originates from the wave height observed by experienced ship captains[22]. H_s can be calculated by zero-crossing analysis $(H_{1/3})$ or through the wave spectrum (H_{m0}), where the latter has become the most common method. Still, the deviation between $H_{1/3}$ and H_{m0} is rarely more than 5% [27]. The significant wave height $H_{1/3}$, is defined in the figure above as the average of the highest one-third of the wave heights within the measurement period [30]. According to the World Meteorological Organization (WMO) [27], the significant wave height should be measured from a wave record which contains at least 200 waves. Knowing that a normal wave can have a downcrossing period T of about 4-12 seconds, a reasonable measurement time is about 15 -

35 minutes[27]. The values of $H_{1/3}$ is therefore usually calculated by using a measurement time of 20 minutes[29].

The significant wave height H_s is accompanied by a characteristic zero-crossing period T_z, which is calculated by averaging the downcrossing period T within the measurement time. The pair H_s, T_z is called a sea state and different sea states will have different impacts on an offshore structure[22]. For some installations, high waves and long periods can be severe, while for others, lower waves and wave periods around the eigenfrequency of the structure is more critical. Therefore, the peak period T_p (see section 3.2.5) is sometimes used instead of T_z[31].

3.2.4 Maximum wave height

Assuming that a wave record follows a Rayleigh distribution, it is possible to calculate the highest expected wave height within the wave record, given a certain H_s. A common way to do this is assuming that[27]:

$$H_{max} = H_s \cdot \sqrt{0.5 \ln \mathrm{N}}, \tag{3.8}$$

where N is the number of waves in the record. For N $\simeq$ 200-1000 waves the value of H_{max} will be around 1.6 - 1.9 the value of H_s. This means that if a measurement of the significant wave height is 12 metres, the highest wave in the wave record can be as high as 23 metres. As a rule of thumb it is reasonable to say that the maximum wave height will not exceed twice the significant wave height ($H_{max} \leq 2H_s$).

3.2.5 The wave spectrum

Because of the theoretical and physical meaning of a ocean surface wave being a sum of sinusoids with different properties, it is possible to transform a time series of wave heights and periods into a frequency spectrum. This is done by Fourier transform, a method used in signal processing. The Fourier transform basically transforms a set of data from the time domain to the frequency domain, the result showing the distribution of the wave energy within the different frequencies. Fast Fourier transform (FFT) is the most common method for processing a time series into an energy spectrum. Several parameters can be derived from the wave energy spectrum $E(f)$, such as the peak period T_p and the significant wave height H_{m0}.

Mathematically, the surface elevation above the mean sea level can be written as[27]:

$$\eta(t) = \eta_0 + \sum_{i=1}^{n} a_i \sin(j\omega_0 t + \phi_j), \tag{3.9}$$

where η_0 is the mean elevation, a is the amplitude, ω_0 is the angular wave frequency of the longest wave fitted to the record, ϕ is the phase angle and i is the number of wave component. If a Fourier transform is performed on a time series of wave height assuming equation 3.9, the wave energy spectrum is obtained. It is also possible to synthesize realistic time series of wave height from a given energy spectrum by using the inverse FFT. An example of an FFT on a

wave height time series is shown in figure 3.5. This type of spectrum is called the omni- or nondirectional spectrum because it does not contain information about dominant wave directions[30].

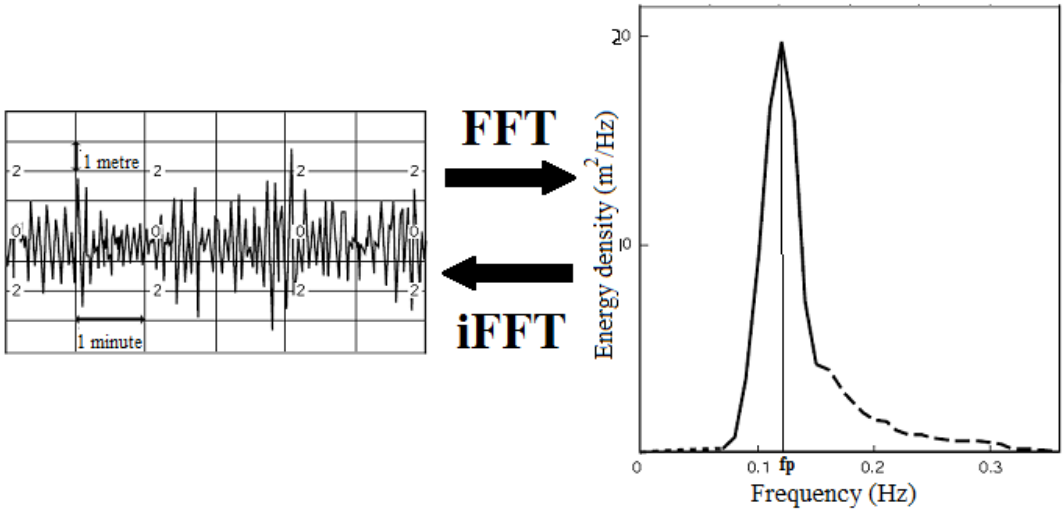

Figure 3.5: *Example of Fourier transform used in wave analysis (Courtesy of WMO)*[27]

The integral under the whole spectrum will give the total variance m_0 of the wave record and also gives the total wave energy (per unit area) by multiplying with $\rho_w g$ (see equation 3.7). The significant wave height is estimated by H_{m0}, which is four times the standard deviation of the wave record[27]:

$$H_{m0} = 4\sqrt{m_0} \tag{3.10}$$

The peak frequency f_p (right figure) is the frequency containing the most energy in the spectrum and is defined through the peak wave period T_p as $f_p = 1/T_p$[30].

Several theoretical wave spectra based on a number of measurements has been developed since the 1950's, like the Pierson-Moskowitz (PM) and JONSWAP (the Joint North Sea Wave Project) spectrum,see figure 3.6. The two spectra describes waves for different sea states and the form of each spectrum depend on factors like wind speed above the ocean and peak frequency[27]. According to IEC 61400-3, which is the International Electrotechnical Committee's standard for wind turbines, both spectra can be used for synthesizing wave height time series, which again works as inputs in models that analyse the loads on the wind turbine structure caused by waves. The same can be done by simulating time series of wind speeds using other spectra describing wind variation. This enables the opportunity to observe the combined structural response on the turbine from wind and waves and discovering potential weaknesses at various conditions.

Improvements of the spectra has been suggested by Torsethaugen[28] by reducing the number of parameters defining the shape of the spectrum to only the significant wave height H_s and

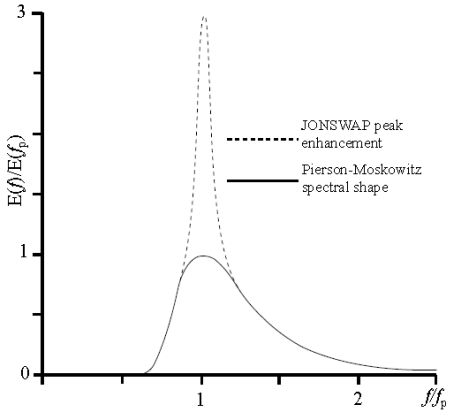

Figure 3.6: *JONSWAP and PM spectra (Courtesy of WMO)*[27]

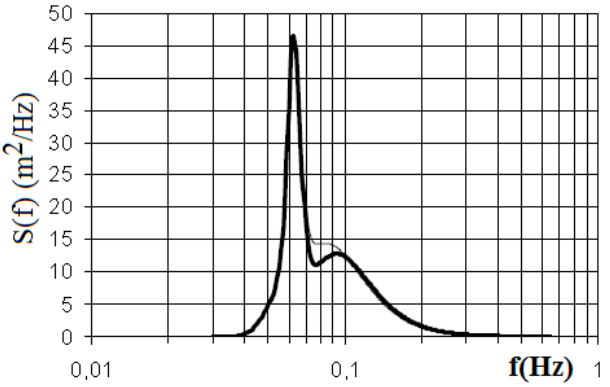

Figure 3.7: *Torsethaugen's spectrum (Courtesy of Knut Torsethaugen)*[28]

the peek spectral period T_p. Torsethaugen's double peak spectrum, unlike the single peak spectrum for PM and JONSWAP, is shown in figure 3.7. The spectrum was in good agreement with wave measurements from Norwegian oil platforms (Statfjord and Gullfaks C)[28]. In simulations of the structural response of a wind turbine one should choose the spectrum which matches the measured spectrum at the location where the wind farm is to be built or from a site resembling this location. It is also possible to run several simulations to see if there are any great differences in load response between the spectra.

3.3 Long-term wave statistics

3.3.1 Variability of significant wave height in space and time

Wave conditions at a certain place on Earth depend on sea depth, distance to shore and wind conditions. Also, it is important whether the place is located in the "shadow" of nearby islands or continents relative to the dominant wave direction. The southern part of the North Sea is an example of this, where waves coming from the Atlantic are absorbed at the west coast of the British Isles. The relatively mild wave climate combined with high wind speeds and low depths is what makes this area attractive for offshore wind power. Other examples of wave shadowing is the Mexico Gulf, the Mediterranean and the west coast of Japan. Figure 3.8 shows the mean significant wave height $\bar{H}_s$ (or $H_{s,mean}$) in the world, where this phenomena is clearly observed.

If data is only available from one geographical location, it could for some applications (see section 4.5) be useful to use wave height measurements from one place (e.g. the North Sea) to represent other places on Earth (e.g. east coast of the United States). This could be executed by scaling the H_s measurements with a factor corresponding to the mean significant wave height for the two locations (e.g. $\bar{H}_{s,UnitedStates}$ divided with $\bar{H}_{s,North\ sea}$). The same principle could be used for wind speed data as well.

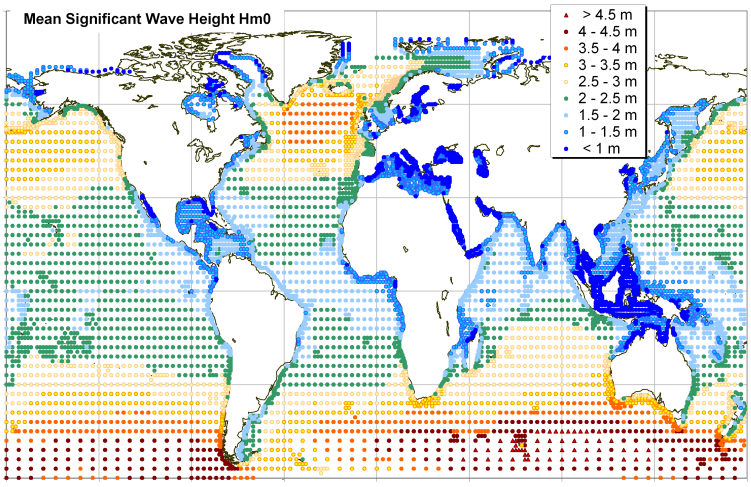

Figure 3.8: *Mean significant wave height in the world. The data originate from the ECMWF (European Centre for Medium-Range Weather Forecasts) WAM model archive and are calibrated and corrected (by OCEANOR) against a global buoy and Topex satellite altimeter database. Courtesy of Stephen Barstow, Fugro OCEANOR AS*[32]

Even though this would be tempting, it is important to mention that although $\bar{H}_s$ for a year is the same at two locations, the probability density function for H_s can look very different. If the deviation from $\bar{H}_s$ is large, the peak of the PDF will be broad, while a small deviation gives a narrow peak. When fitting several years of H_s measurements to a certain distribution function, the shape of the PDF is determined by a parameter describing the deviation from $\bar{H}_s$, like the shape factor β for the Weibull distribution, see section 3.3.2. If scaling of wave and wind data is necessary, knowledge about the parameters controlling the PDF at the desired location is vital in order to get realistic results.

The variability of wave heights in time highly depends on the variation of wind speed throughout the year. In the North Atlantic Ocean (and also the North Sea and Norwegian Sea), wind speeds are higher in winter and lower in summer. The wave height will normally follow the same pattern, causing more rough sea in the winter months[33]. The high correlation in mean wind speed and mean significant wave height for the Sleipner A platform in the North Sea can be observed in figure 3.9.

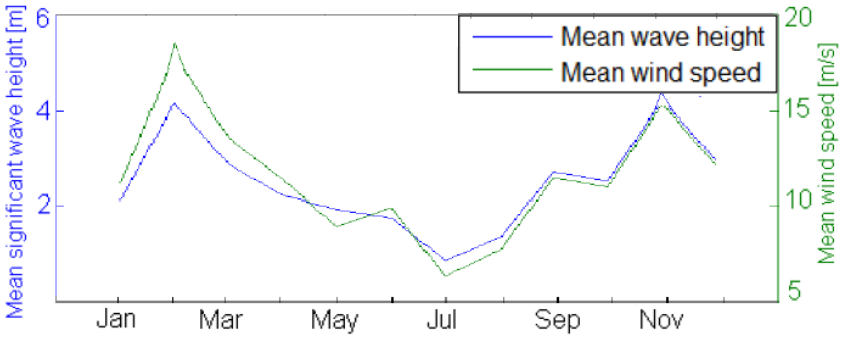

Figure 3.9: *Montly mean significant wave height and wind speed for Sleipner A platform in the North Sea, 1997*

3.3.2 Long-term signficant wave height distributions and extreme wave statistics

Measurements of H_s over several years tend to follow certain statistical distributions, but which distribution that fits the data best depends on the location where the data is collected. Well used distributions are the log-normal, the Weibull and the Fisher-Tippett (i.e. extreme value) distributions. When fitting a data set of H_s to a distribution, it is possible to plot 1) the probability density function (PDF) and 2) the cumulative probability distribution. The 2-parameter Weibull PDF is given as[27]:

$$f(H_s) = \frac{\beta}{\alpha}\left(\frac{H_s}{\alpha}\right)^{\beta-1} e^{-(H_s/\alpha)^{\beta}}, \tag{3.11}$$

where β is the shape factor and α is the scale factor. A Weibull fitting of data from the Draugen platform for 2000-2005 is shown in figure 3.10.

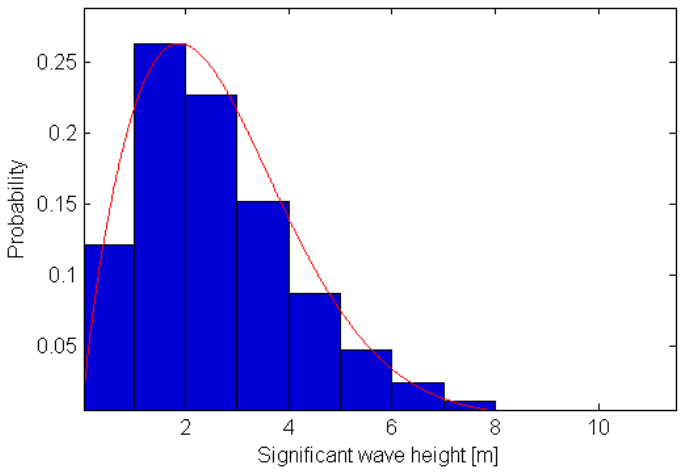

Figure 3.10: *Probability density histogram vs. Weibull PDF plot with scale factor α = 3.02 and shape factor β = 2.67. Data from Draugen platform 2000-2005*

The cumulative probability distribution shows the probability of a value of H_s not exceeding a certain value, which can be used for extreme value analysis. By using data for a few years it is possible to estimate the highest significant wave height that will occur within a given time period referred to as the return period. The return period can be 50,100,1000 or 10000 years and H_s for a certain return period is denoted H_{s50}, H_{s100}, H_{s1000} etc.

The method is first to calculate the non-exceedance probability for the given return period, which can be done by[27]:

$$P(Hs < H_{T_r}) = 1 - \frac{1}{(\text{Number of Hs values in a year}) \cdot T_r} \tag{3.12}$$

where T_r is a given return period. For a return period of 50 years using measurements of H_s every three hours (365.25 x 8 per day = 2922), the non-exceedance probability is calculated to be 0.999993. The next step is to choose a distribution for which the data can be fitted to.The

Fisher-Tippett Type I (FT-I), also known as the Gumbel distribution, can be used for extreme value analysis has a cumulative probability distribution function given as [27]:

$$F(H_s) = exp(-exp(-\theta(H_s - \epsilon)),$$
$$\theta = \frac{\pi}{\sqrt{6\sigma_{Hs}^2}}, \quad \epsilon = \bar{H}_s - \frac{0.5772}{\theta}, \tag{3.13}$$

where σ_{H_s} is the standard deviation of the mean significant wave height $\bar{H}_s$ The extreme value can be calculated by solving 3.13 with respect to H_s. A graphical approach is to plot the cumulative probability distribution on a probability paper, where the y-axis is logarithmic[27]. This is performed in figure 3.11, where it becomes clear that the extreme value calculation is really an extrapolation of measured data.

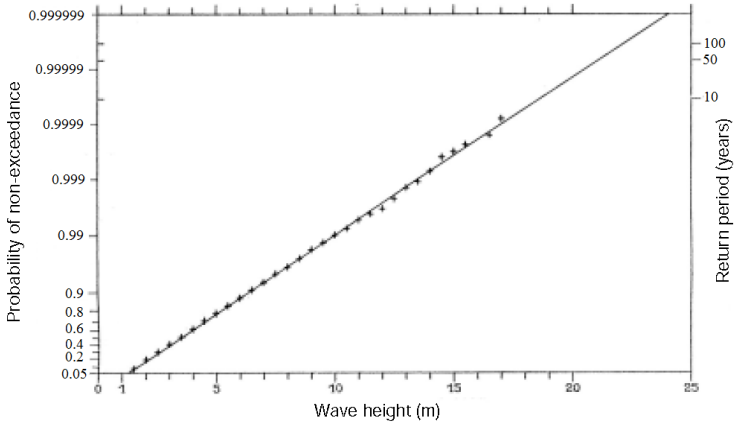

Figure 3.11: *Calculation of extreme H_s is performed through the cumulative probability distribution. Data from the Weather Ship Lima, Dec 1975-Nov 1981 (Courtesy of WMO)* [27]

Naturally, there will always be some degree of uncertainty when calculating extreme signficant wave heights. Finding a distribution that fits the data well is therefore important to avoid large errors in the extreme value calculations. According to Knut Iden at the Norwegian Meteorological Institute (DNMI), *"the GEV (Generalized extreme value) and GP (Generalized Pareto) distributions are used when performing calculations of extreme wave heights on Norwegian offshore installations. Both methods rely on an independent set of data and one should ideally have a time series which has a length of at least a third of the return value one wishes to calculate.[34]"*. If it is necessary to calculate the peak period T_p associated with an extreme significant wave height as well, one has to fit the data to a joint probability density function, which describes probabilities for a H_s-value given a certain T_p. The extreme value calculation is performed by extrapolating the data in two dimensions (the H_s,T_p-space) to the desired return period. This is described in [29] and performed more in detail in [31].

3.3.3 Wave forecasting

The forecast for waves is obviously important for fishing boats and shipping industry, but also for offshore installations in case of the need for evacuation of personnel. National and

international weather services executes forecast for different regions of the ocean by using wave models. The Norwegian Meteorological Institute performs a forecast with a period of 66 hours for a large area stretching from the Barents Sea to the Atlantic, see figure 3.12. The model used by DNMI is called WAM, which is a spectra wave model developed in 1994 that uses wind data from a larger model called HIRLAM as input. WAM50 is run with a 50 km resolution four times a day, while WAM10 (10 km) and WAM4 (4 km) is run twice a day. Additionally, the model SWAN (Simulating Waves Nearshore) is utilised to forecast waves for some coastal regions of Norway (Karmøy and Trondheimsleia)[35]. A snapshot of a forecast outside the Norwegian coast is shown in figure 3.13:

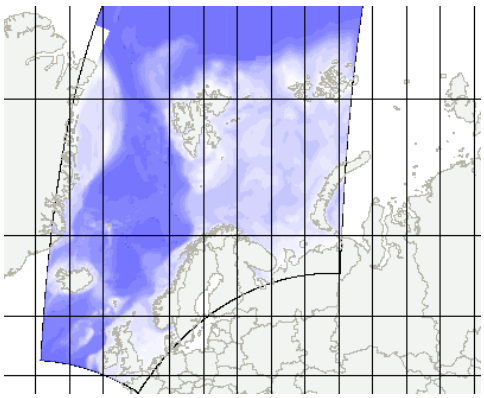

Figure 3.12: *Area of wave forecasting performed by DNMI*[36]

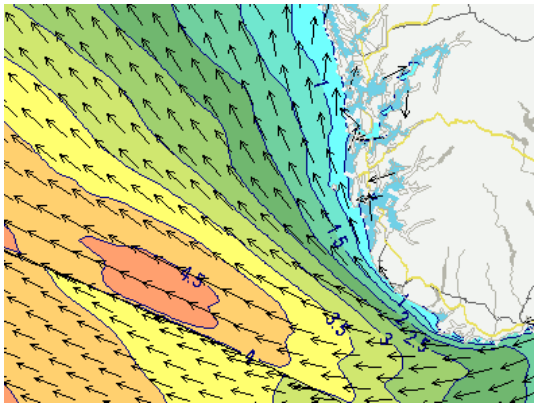

Figure 3.13: *Example of significant wave forecast outside Norwegian coast*[37]

Although models for wave forecasting are constantly improving, it is very difficult to predict significant wave heights exactly. To validate how well a wave model predicts wave heights, it is possible to compare forecasts with actual buoys on a certain location. This is done by DNMI in [35]. Statistical parameters used for this validation is the bias and the root mean square error (RMSE) and bias, where the first gives information whether the forecast exaggerates or underestimates the wave height and is calculated by[35]:

$$\text{BIAS} = \frac{1}{N}\sum_{i=1}^{N}(H_{s,i}^{forecast} - H_{s,i}^{measurement}), \tag{3.14}$$

where N is the number of measurements/forecasts. In words, the bias is just the mean deviation between a forecast and a measurement. One should be aware that although the bias is an useful parameter for many purposes, a bias value of zero does not necessarily mean that a forecast model is perfect. It should therefore be accompanied by the RMSE, which is calculated by[35]:

$$\text{RMSE} = \sqrt{\frac{1}{N}\sum_{i=1}^{N}\left(H_{s,i}^{forecast} - H_{s,i}^{measurement}\right)^2} \tag{3.15}$$

The time series of bias and RMSE for the forecast of H_s in the North Sea and Norwegian Sea from 1999-2011 is shown in figure 3.14. The different colors indicates different lead times, from 0 hours (nowcasting) to 48 hours ahead in time.[35]

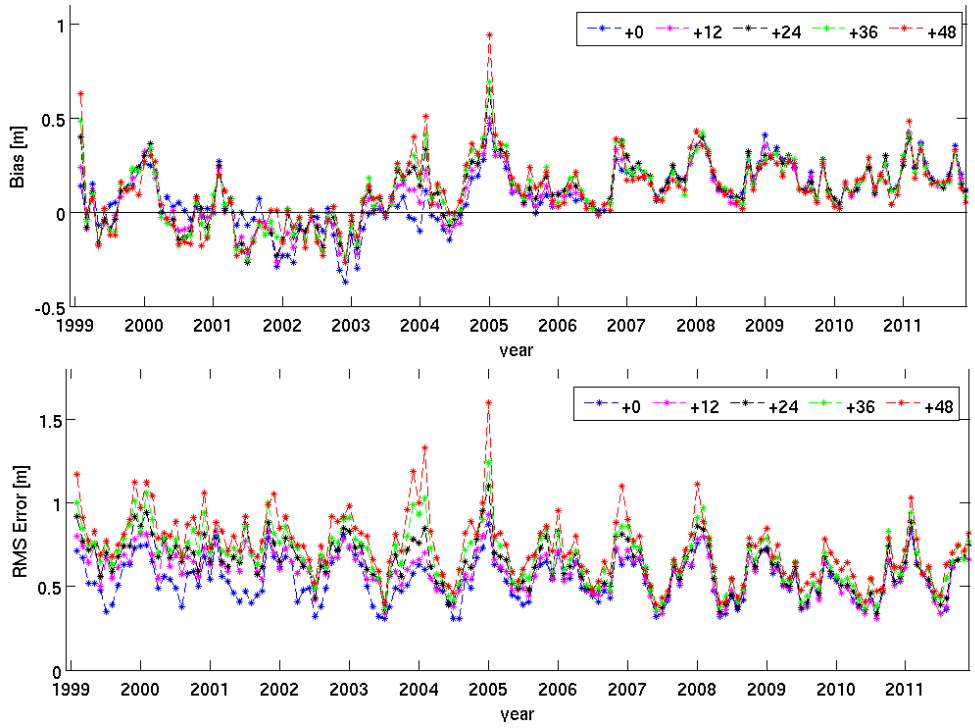

Figure 3.14: *Time series of bias and RMSE in North Sea and Norwegian Sea 1999-2011 (Courtesy of Yvonne Gusdal,DNMI)*[35]

In the time series of bias one can observe that the forecast has been steadily overestimating H_s in the same pattern for all lead times since 2007, when WAM10 was implemented. Another observation is that the bias varies from 0.1 m in summer up to 0.5 m in winter. This is because the wave model is less accurate for high wave heights ($H_s > 4.0m$), which occur more frequently in winter. The same seasonal pattern is observed in the time series of the RMSE.

[35] calculated the False Alarm Ratio (FAR) for different wave heights and lead times, meaning the fraction of forecasted events that did not happen. For all lead times (also nowcasting) with waves in the range of 6-8 metres the FAR could be about 50%. This means that the only half of the forecasted wave heights in this range actually occurred. In general, the deviation in bias between the different lead times is not very large; for many cases, a 24-hour forecast might be just as good as a 12-hour forecast.[35]

[35] also found that *" the limited area wave model from ECMWF (European Centre for Medium-Range Weather Forecasts) run at 11 km resolution (WAMECMWF), has a better score than all wave models at met.no. The WAMECMWF is a coupling between the atmospheric and wave model, while for WAM at met.no there is no coupling. The lack of wave-atmospheric coupling excludes important dynamics, and may be the reason for the higher score for the ECMWF model compared to wave models at met.no (DNMI)"*. In November 2011 an enhancement of the wave height of 4% for winds between 15 m/s and 25 m/s was removed[35]. If the improvement will reduce the positive bias and the false alarm ratio of the model will first be answered when the validation report for the year 2012 is made[38].

3.3.4 Global warming impact on wave heights

Several studies has been done to investigate whether global warming could lead to higher wave heights in the future. This is problematic since higher wave heights would cause more erosion and flooding[39]. Also, higher extreme wave heights could have great consequences for offshore and shipping industry if the increase is higher than the safety limits which are constructed into the design of ships and offshore structures[40]. For offshore wind farms with a life expectancy of 20-30 years, it would be important to know how much the wave height and wind speed is expected to rise within the life time.

Magnar Reistad[40] at DNMI found an increase in extreme wave heights in the North Sea and the Norwegian Sea of 0.25-0.5 m and 1-1.5 m respectively, within a time period of roughly 50 years (1955-2000). $H_{s,100}$ in the northwestern part of the Norwegian Sea was estimated to increase with almost two metres, which is more than 10%. Another study performed by Ian Young et al. at the Swinburne University of Technology, Australia found that for the time period 1991-2008, *"there has been a consistent trend toward increasing wind speeds over seas all around the world. For wave height, there is no clear trend for mean monthly values. At more extreme conditions (extreme wave height) there is a statistically significant trend of increasing wave height at high latitudes and more neutral conditions in equatorial regions"*[41]. Both studies emphasizes that there are great uncertainties related to the estimates, as with all possible effects from global warming.

Chapter 4

Materials and methods

This chapter describes the approach to reach the objectives defined in the introduction of this master's thesis. Ideally, the method should explain the thesis work in a way that it can be reproduced by others without exaggerating the level of detail. This has been solved by using flow diagrams and concrete examples from the data analysis from one or several sites. In addition, the complete script and raw data used in the thesis is available electronically. Although the main results concerning the thesis objectives are placed in the next chapter, some preliminary results are presented here where this has been considered necessary to understand the further process of the method.

The outline of the method is described in the flow diagram below:

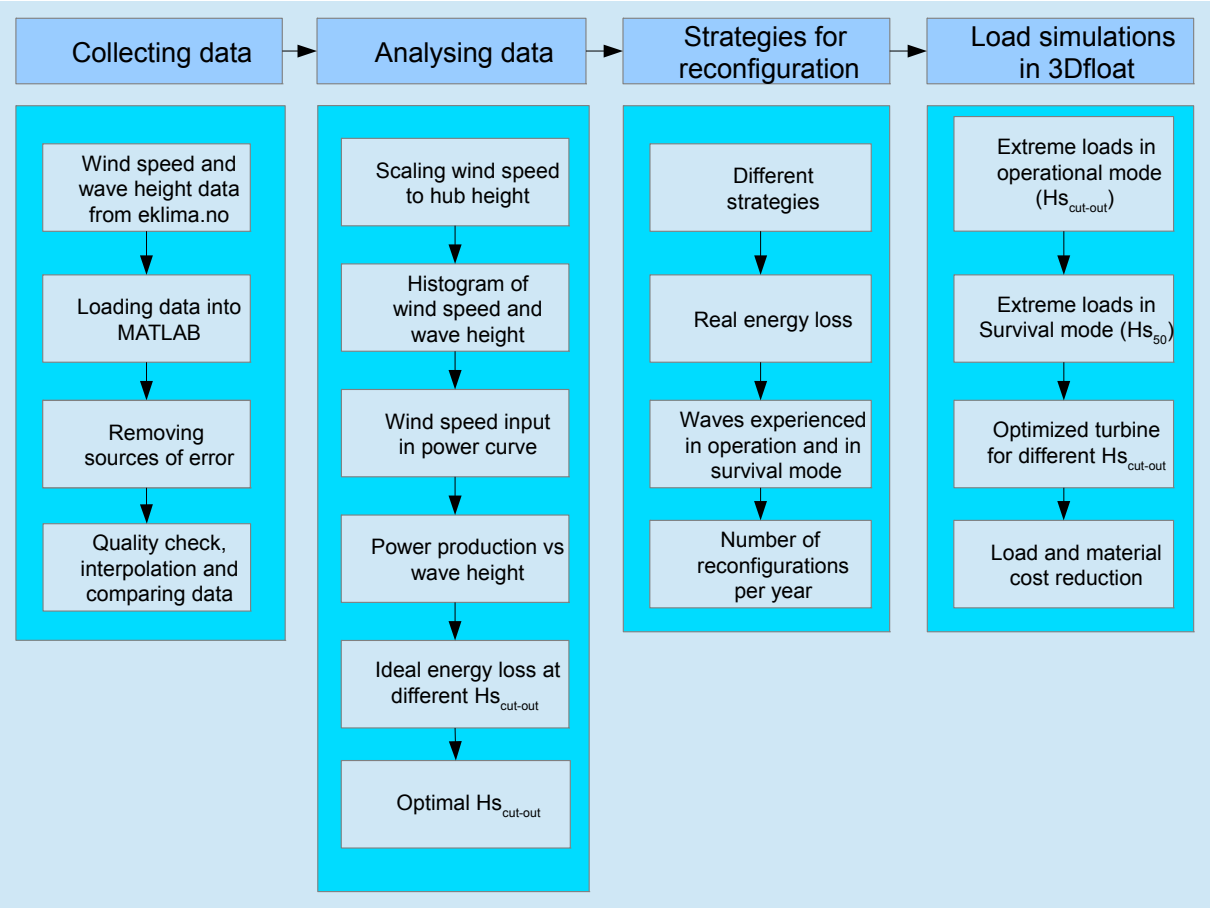

Figure 4.1: *Flow diagram of the method used in the thesis*

As it can be seen in figure 4.1, the method consists of four main blocks that will be explained more in detail in this chapter. In addition to these four, a sensitivity analysis and a scaling of the data to fit other floating wind power markets has also been performed.

4.1 Collecting data

4.1.1 Wind speed and wave data from eklima.no

The wind speed and wave height data used in the thesis has been collected from eklima.no[42], which is the Norwegian Meteorological Institute's on-line database for free weather data. The database contains data gathered from meteorological stations that have been or are still in operation, including measurements from offshore oil platforms in the Norwegian and North Sea. All data has gone through a quality control by the DNMI, but systematic error still might occur (e.g obstacles disturbing wind measurements).

Data was collected from the oil platforms Ekofisk, Sleipner A, Heimdal, Gullfaks C, Draugen, Troll A and Heidrun, in addition to the ship Norne, for as many years as possible. Although a number of parameters was available, like wind and wave direction, wave period, maximum wave height etc., only two parameters was considered relevant for this thesis:

- u - Wind speed 10 metres above ground averaged over 10 minutes
- H_s - Significant wave height (measurement time: 20 minutes)

The data was available with a measurement interval of 20 minutes, meaning that in a year, each site would have 26280 measurements for each parameter. Since several years of measurement was collected, the large amount of data called for a different processing tool than Excel. Due to the prior knowledge of the program, MATLAB was chosen. Information about the oil platforms are given in table 4.1:

Table 4.1: Oil platforms with meterological measurements [43, 44]

	Depth	Shore distance	Measured since	Anemometer height (red. factor)
Ekofisk	75 m	263 km	1980	116 m (0.73)
Sleipner A	82 m	199 km	1993	137 m (0.71)
Heimdal	120 m	152 km	2003	73 m (0.776)
Troll A	300 m	70 km	1998	94 m (0.74)
Gullfaks C	216 m	121 km	1989	143 m (0.71)
Draugen	251 m	63 km	1993	78 m (0.77)
Heidrun	350 m	155 km	1995	131 m (0.71)
Norne (ship)	380 m	152 km	1998	$\simeq$ 60 m (0.8 - 0.84)

The wind sensors are placed as unexposed to obstacles as possible, which means that they are often placed on the top of the drilling tower[34]. The reduction factor is used to estimate the wind speed 10 metres above sea level by multiplying it with the wind speed originally measured at the anemometer. Figure 4.2 shows the placement of the measurement stations.

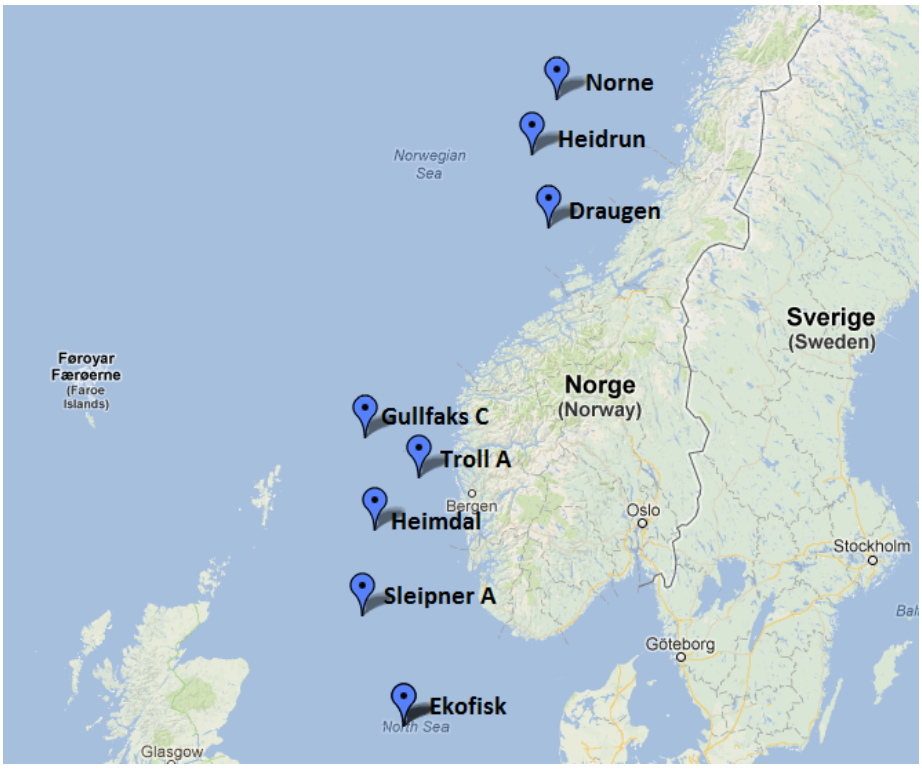

Figure 4.2: *Map over measurement stations*[42]

As it can be seen in table 4.1 and figure 3.8, the stations represent a cross section of different wave climates, ocean depths and distances to shore. The shallow depths in the south part of the North Sea combined with a wave shadowing effect from the British Isles leads to a relatively mild wave climate at Ekofisk compared to the rougher climate in the Norwegian Sea (Draugen, Norne and Heidrun). The oil platforms in the northern part of the North Sea (Gullfaks C, Troll A, Heimdal and Sleipner A) have wave climates somewhere in between Ekofisk and Heidrun.

4.1.2 Removing sources of error

In the gathered time series of $u(t)$ and $H_s(t)$, there were some data missing, sometimes for several weeks at a time and other times for only a few hours. The reasons for missing data can be many, like malfunction or maintenance of a wave buoy or wind anemometer. Due to the variation of wind speed and wave height throughout the year, one cannot simply ignore the missing data in the analysis, since this may lead to unrealistic calculations of energy production and errors in the wave height distribution. This was dealt with by manually controlling the wind and wave data by plotting the time series in MATLAB and looking for

missing data ($u(t)$ and $H_s(t) = 0$). In the years where several weeks of data was missing at a time or the data quality looked poor in general, the whole year of data was removed. A more professional way to do this is hindcasting, where data from wave models in combination with other nearby measurement stations is used to fill in the data. This, on the other hand, was considered out of scope in the thesis due to the possibly lengthy process of learning to do this from scratch.

Another source of error is the lack of homogeneity, which means that the mean wind speed or mean H_s changes radically in the years observed. The assumption of an homogeneous data set is important for any results in the thesis. Although a thorough homogeneity test was not performed, simply plotting the time series of the wind and wave data and checking for stability of the means across time revealed that the wind speed data from Norne was erroneous. Measurements from Norne was therefore excluded in further data analysis.

A study on the potential of ocean energy in Norway made for Enova SF [45] contains energy production calculations using wind speed data from the same measurement stations used in this thesis. The part of the study containing offshore wind energy is written by Kjeller Vindteknikk. [45] discusses uncertainties related to wind speed measurement due to disfavourable placements of the wind sensors and mentions that measurements from Troll A seem to be less reliable for some wind directions. For this reason, Troll A was also removed from further analysis.

4.1.3 Quality control and interpolating missing data

After the removal of two complete measurement stations and several years at the remaining stations, a quality control of the data was performed. This included calculating the valid percent, which is the proportion of a sample that is valid(i.e not missing). In addition, the length and frequency of missing data was calculated for both wind speed and significant wave height. A total quality assessment of the data was performed by giving each site a quality grade of very good, satisfactory or uncertain, see table 4.2.

Table 4.2: Validation and quality assessment of data

	Years of valid measurements	Valid percent H_s	Valid percent u	Quality grade
Ekofisk	1997,2002-2003,2006-2007	92.3% (15 days)	96.7% (4 days)	Satisfactory
Sleipner A	1995-1999, 2001-2006, 2008-2012	87.8% (22 days)	98.2% (7 days)	Uncertain
Heimdal	2004-2009	97.1% (5 days)	98.5% (5 days)	Very good
Gullfaks C	1997-2000,2007-2009	93.7% (12 days)	98.3% (7 days)	Very good
Draugen	2009-2012	87.2% (5 days)	99.4% (16 days)	Satisfactory
Heidrun	1997-1999,2001,2004-2012	93.0% (5 days)	96.0% (5 days)	Satisfactory

The number in the parenthesis behind the valid percent is the maximum days of missing data at a time. There are more missing H_s data than wind speed data for all the stations. Still,

due to the slower temporal variation of waves compared to wind, it is less problematic to interpolate several days of wave heights. The interpolation of the missing wind and wave data was necessary before the data could be analysed further. This was done by using the cubic interpolation function in MATLAB, which unlike a linear interpolation makes a smooth and more realistic curve between two existing data points. Nevertheless, the interpolation leads to some uncertainty, especially for sites with long periods of missing data.

To check if the remaining data gave realistic results even after the interpolation, the estimates of mean wind speed and annual energy production from the Enova report [45] have worked as a control reference. The report calculates the wind speed in hub height (u_{hub}) and uses this as input for the power curve of a Vestas V90-3.0 MW turbine[15] with a hub height of 90 metres, cut-out wind speed of 25 m/s and a re cut-in speed of 20 m/s. By following the same procedure as [45] (method for calculations of u_{hub} and energy production explained more thoroughly in section 4.2), it was possible compare the results from using the thesis data with the estimates from [45]. An overview over the results are shown in table 4.3.

Table 4.3: Comparison of thesis data with Enova report[45]

	Number of years (Time period)		Mean u_{hub} (m/s)		AEP (GWh)	
	Enova	Thesis	Enova	Thesis	Enova	Thesis
Ekofisk	27 (1980 – 2007)	5 (1997 – 2007)	10.9	9.6	14.3	13.5
Sleipner A	14 (1993 – 2007)	16 (1995 – 2012)	11.1	11.2	14.5	14.5
Heimdal	N/A	6 (2004 – 2009)	N/A	10.8	N/A	14.0
Gullfaks C	17 (1989 – 2007)	7 (1997 – 2009)	11.2	11.1	14.1	14.3
Draugen	14 (1993 – 2007)	4 (2009 – 2012)	10.4	9.6	12.8	12.3
Heidrun	12 (1995 – 2007)	13 (1997 – 2012)	10.0	10.3	N/A	13.1

The comparison shows good agreement for the mean u_{hub} and annual energy production at Gullfaks C and Sleipner A, while there are some deviations for Ekofisk and Draugen. No more data sets were removed after the quality assessment and comparison with the Enova report and the data analysis could begin.

4.2 Analysing data

4.2.1 The wind farm

In this thesis, one TLB B turbine is considered to experience the wind and waves measured at the different oil platforms. Still, the perspective of the research group led by Tor Anders Nygaard is that a large wind farm consisting several hundred turbines is constructed. One example is a wind farm with 100 turbines that would be placed in an area of 9 $\times$ 9 km with a distance of 1 km between each turbine, see figure 4.3.

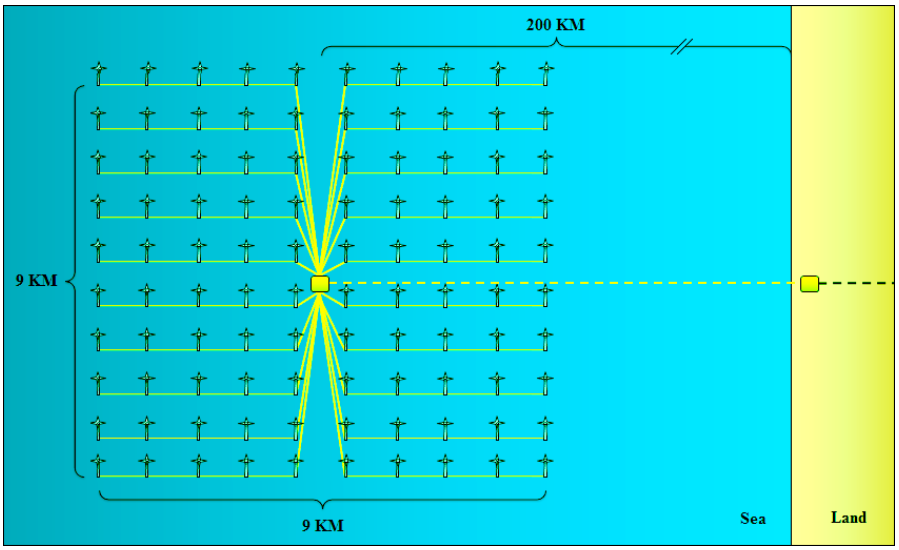

Figure 4.3: *Geometry of TLB wind farm with 100 turbines*[46]

The turbines are assumed to experience the same wind speed (no wake losses) and wave height, only separated in time depending on the turbine distance and wind/wave speed. Including wake losses and energy loss at different $H_{s,cut\text{-}out}$ for the whole wind farm is a more complicated matter since wake models and wind directions would have to be included. This was considered beyond the scope of this thesis due to time limitations and one TLB B turbine is therefore assumed to represent the whole wind farm, both for energy loss and turbine loads.

4.2.2 Scaling wind speed to hub height

Since wind speed measurements are available at a height of 10 metres ($u_{10\text{ m}}$) and the height of the turbine tower of the TLB B and many other offshore wind turbine towers are usually around 90-100 metres tall[5], the wind speed must be scaled up to hub (nacelle) height Z_{hub}. A clever way to do this is to follow the same procedure as described in [45]. First, the wind speed originally measured at the anemometer height $Z_{anemometer}$ is calculated by dividing on the reduction factor given in table 4.1. Then the hub height wind speed u_{hub} is estimated by assuming a power law profile given in equation 2.2.

u_{hub} can be calculated directly by using the following equation:

$$\begin{aligned} u_{hub} &= u_{anemometer} \cdot \left(\frac{Z_{hub}}{Z_{anemometer}} \right)^{\alpha}, \\ u_{anemometer} &= \frac{u_{10\text{ m}}}{\text{red. factor}} \end{aligned} \tag{4.1}$$

The shear exponent was assumed to be $\alpha = 0.1$, while a hub height of $Z_{hub} = 90$ m was chosen.

4.2.3 Wind speed and significant wave height distributions

After collecting, controlling and comparing data, time series from each site of u_{hub} and H_s was available. These time series have been analysed and processed through several steps before the

optimal cut-out wave height could be chosen for the specific measurement station. Figures and results from Sleipner A are used as examples to explain more easily how the processed time series from the different sites look like.

To start with, the coherent time series of u_{hub} and H_s was plotted and distributions similar to that in figure 3.10 was made by using MATLAB's histogram function, see figure 4.4.

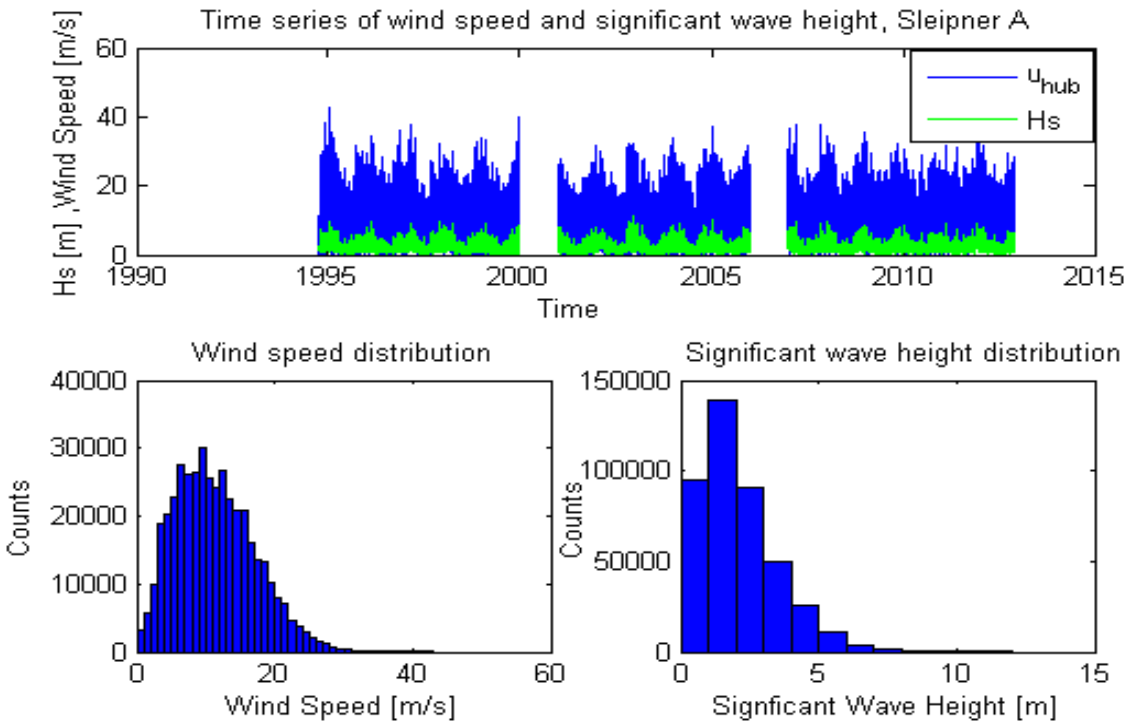

Figure 4.4: *Time series and distributions of u_{hub} and H_s for Sleipner A*

The next step was to investigate the coherence between u_{hub} and H_s by making a joint histogram. Figure 4.5 shows a three-dimensional histogram observed from above that has been smoothed out and coloured to illustrate where the measurements are located. Although the correlation between wind and waves is high, there are several events where there are high wind speeds and low wave heights and vice versa.

Introducing a cut-out wave height for a floating wind turbine will therefore have an impact on the energy production of a wind farm, as illustrated in figure 4.6. For a common wind turbine with a cut-out wind speed of 25 m/s, all wind speeds above this limit is "lost wind", highlighted in red and light blue. If a survival mode system makes the turbine shut down at $H_{s,cut\text{-}out} = 8$ m, there are events where the wind speed is below $u_{cut-out}$ (highlighted in green) and the turbine would otherwise produce energy. The first objective of this thesis is to find the loss in energy production when varying the $H_{s,cut\text{-}out}$.

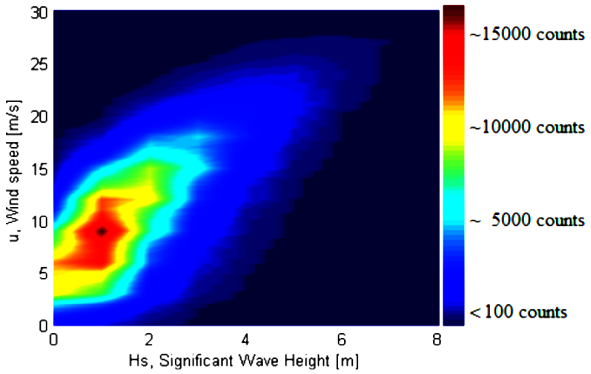

Figure 4.5: *Joint 3D-histogram of u_{hub} and H_s, Sleipner A*

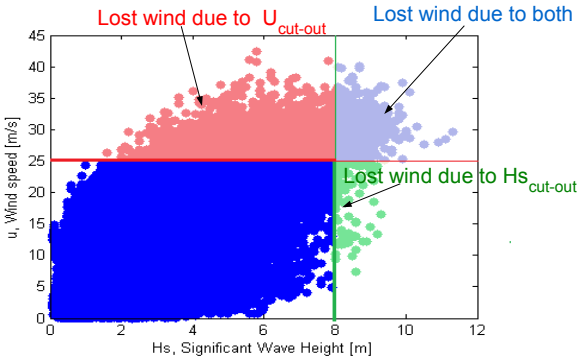

Figure 4.6: *Impact of $u_{cut-out}$ = 25 m/s and $H_{s,cut\text{-}out}$ = 8 m, Sleipner A*

4.2.4 Power curve and energy production

To simulate the energy production of the TLB B for each site, a turbine had to be chosen. The power curve from the NREL 5 MW turbine was selected (see figure 2.2), which has a hub height of 90 metres[11]. The turbine cuts in at 3 m/s, cuts out at 25 m/s and re cuts-in when the wind speed drops below 25 m/s, meaning that the turbine is assumed to be dead band controlled unlike the high wind hysteresis control used in the Vestas V90.

By inserting u_{hub} into a power curve table containing power output in kW at different wind speeds, a time series of power output $P(t)$ from the wind turbine could be produced. The power output was assumed to be constant within the measurement time (20 minutes) and the energy output for this period in kWh was calculated by multiplying the power output with the measurement time in hours ($\frac{20\text{min}}{60\text{min}} = \frac{1}{3}$ h). The total energy output was calculated by summing the individual energy outputs using equation 2.3 and the effect of introducing the $H_{s,cut\text{-}out}$ could now be investigated.

4.2.5 Ideal energy loss due to $H_{s,cut\text{-}out}$

If one first assumes that the survival mode system can be switched on immediately, it was possible to calculate the ideal energy loss due to the $H_{s,cut\text{-}out}$. This was easily done in MATLAB by finding all indices where $H_s > H_{s,cut-out}$ and setting the power output at these moments equal to zero. An easy way to illustrate the consequence of this is to make a histogram of energy output versus significant wave height with and with-out the $H_{s,cut\text{-}out}$. This is done in figure 4.7 where the red part shows the lost energy if $H_{s,cut\text{-}out}$ = 6 m.

It is more convenient to use the energy loss in percentage instead of GWh when comparing energy loss to the load reduction achieved with the survival mode system. This is plotted for the different cut-out wave heights in 4.8. If one accepts an energy loss of up to about 1%, a reasonable cut-out wave height for Sleipner A seems to lie in the range of between 6 and 8 metres.

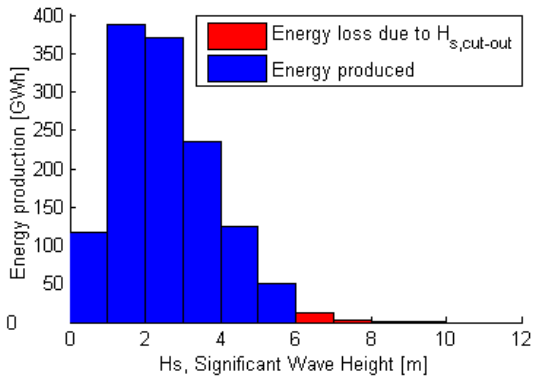

Figure 4.7: *Histogram of energy production vs. H_s with $H_{s,cut\text{-}out}$ = 6 m, Sleipner A*

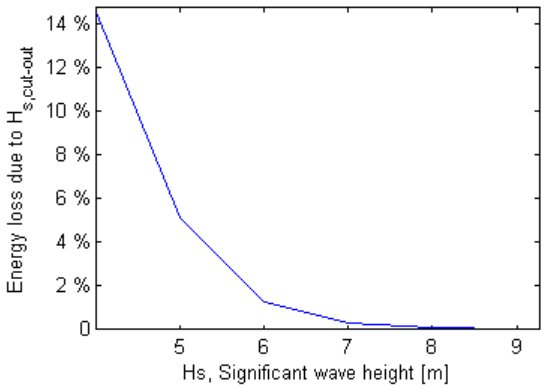

Figure 4.8: *Ideal energy loss in percentage at different $H_{s,cut\text{-}out}$, Sleipner A*

4.2.6 Sensitivity analysis

A sensitivity analysis is performed when one wishes to investigate the uncertainty of an output if one or several input parameters are changed. In this thesis, there are especially two input parameters that affects the energy loss at a given $H_{s,cut\text{-}out}$. The first parameter is the wind speed data, which contains an uncertainty due to the few years of collected data for some sites (see table 4.2 and 4.3) or systematic errors in measurements. The second parameter is the choice of the wind turbine's power curve and control strategy. Although the power curve for the NREL 5 MW turbine with a dead band controlled control strategy is chosen, the Vestas V90 operates with a high wind hysteresis, re-cutting in at 20 m/s. In the future, more offshore turbines will be equipped with a storm control/high wind ride through system operating with a cut-out wind speed of 30 m/s (section 2.2.2). The impact of changing these parameters should be investigated and answer the following questions:

1. What is the effect of increasing or decreasing the wind speed data by a certain percentage?
2. What if other power curves and control strategies are used?

To answer the first question, the wind speed data was simply multiplied or divided by a factor (10% increase $\rightarrow u_{hub} = 1.1 \cdot u_{hub}$, 10% decrease $\rightarrow u_{hub} = \frac{u_{hub}}{1.1}$) and the ideal energy loss was found for the different $H_{s,cut\text{-}out}$. 10% was chosen since this was the maximum deviation in mean wind speed between the Enova report and the data used in the thesis, see table 4.3. To answer question two, the energy loss was calculated by using the power curves of the Vestas V90 with high wind hysteresis and Enercon's E-126 with storm control, see figure 2.2.

4.3 Control strategy for reconfiguration of wind turbine

4.3.1 The need for a control strategy

Section 4.2 focused on finding the energy loss from shutting down the turbine at high waves assuming the reconfiguration into survival mode can be done momentarily. Nevertheless, this

is not entirely realistic. While the rotor in a wind turbine can be stopped within a few moments if the wind speed exceeds the cut-out wind speed, the reconfiguration into survival mode is a more lengthy process. The fact is that no matter which survival mode system is implemented in the TLB B (reconfiguration of mooring lines, ballasting the floater or others), the reconfiguration process could take up to one hour. At the same time, measurements showed that there are numerous events where $H_s(t)$ oscillates rapidly around $H_{s,cut\text{-}out}$. This calls for a control strategy which should fulfil the following criteria:

1. Minimize the energy loss due to introducing the $H_{s,cut\text{-}out}$.
2. Make sure the turbine is in survival mode when high waves occur.
3. Avoid that the survival mode system turns on and off rapidly due to a oscillating $H_s(t)$ around the $H_{s,cut\text{-}out}$.

In this thesis, three main control strategies for the survival mode system have been designed, assuming a reconfiguration time of 20, 40 and 60 minutes (case a), b) and c)). The functionality of the control strategies was measured by how well they fulfil the criteria above. In addition, a few other control strategies which has not been implemented in the model and simulations were looked into and discussed.

To illustrate how the various control strategies operate, the time series of $H_s(t)$ for one particular day at Draugen assuming a $H_{s,cut\text{-}out} = 7$ m has been used as an example, see figure 4.9. This illustrates how each control strategy copes with $H_s(t)$ oscillating around $H_{s,cut\text{-}out}$ and a rapidly decreasing $H_s(t)$.

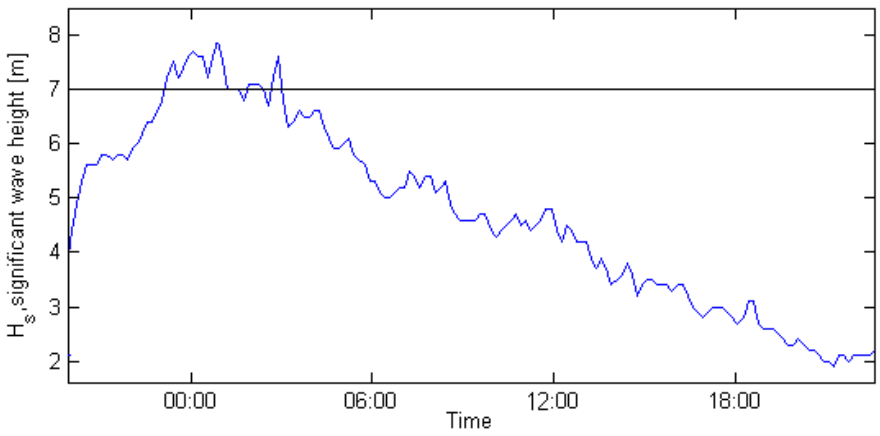

Figure 4.9: *One day time series of $H_s(t)$ from Draugen*

4.3.2 Strategy 1 - Re cut-in wave height

A fairly easy control strategy for the survival mode system is inspired by the high wind hysteresis system which is used for several turbines, including the Vestas V90. If one assumes that a wave buoy is located in the wind farm and measures H_s every 20 minutes, the turbine

shuts down and the survival mode system turns on as soon as $H_s > H_{s,cut-out}$. The turbine will not go back into operation until a H_s measurement falls below the re cut-in wave height $H_{s,re\ cut-in}$. This limit should be low enough to avoid that the survival mode system turns on and off rapidly, but without being too conservative. Through trial and error, a reasonable value of the re cut-in wave height was found to be about $H_{s,re\ cut-in} = H_{s,cut-out}$ - 2 m. An illustration of strategy 1 is shown in figure 4.10.

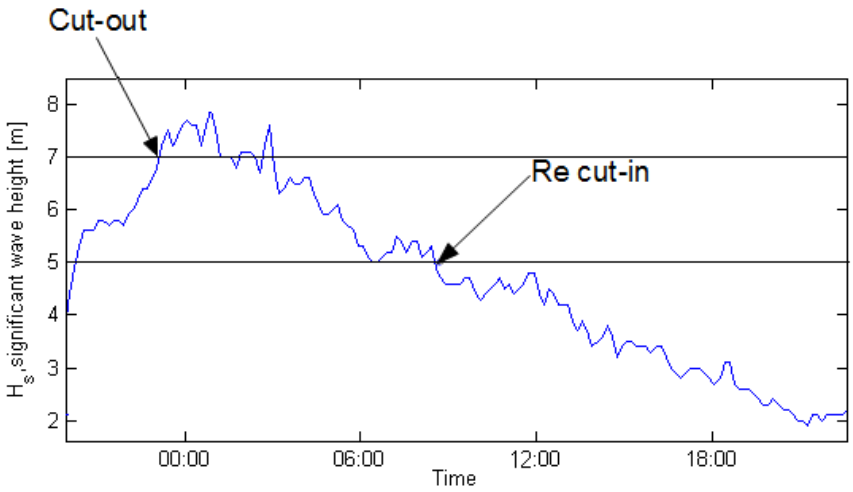

Figure 4.10: *Strategy 1a) with* $H_{s,cut-out} = 7\ m$ *and* $H_{s,re\ cut-in} = 5\ m$

The strategy could easily be implemented in MATLAB by using *for* and *if* loops, setting the power $P(t) = 0$ when the turbine was in survival mode. The energy loss assuming different reconfiguration times, case 1a), 1b) and 1c), was simulated. It was important to remember the fact that when the turbine reconfigures back to operational mode, the turbine will not resume producing energy before the mooring lines are in their original position/the water is pumped of out the floater. A delay equal to the reconfiguration time must therefore be inserted in the energy production calculation for each case. The same delay had to be inserted when calculating the highest wave which the turbine experiences in operational and survival mode.

4.3.3 Strategy 2 - Combining forecast and measurements

Another strategy is to combine measurements and wave forecasting, which might be a safer and more efficient way to control the survival mode system. Section 3.3.3 gives information about the accuracy of wave forecasting, which has been steadily increasing with the use of better wave models. The wave model used by DNMI seems to have a maximum bias of 0.5 metres within a year, but as the bias is only an average of the deviation between forecast and measurement, individual forecasts can have higher errors than this. This was discussed in a meeting with two meteorologists at Kjeller Vindteknikk in April 2013 [47].

They both emphasized that the uncertainty in wave forecasting can be large and claimed that errors of up 1 - 2 metres might occur at specific meteorological conditions where the wind

speed and wave height suddenly increases. These rapid changes can be hard for weather models to pick up and wave forecasting can't always be trusted. This is especially true for the WAM model used by DNMI since it lacks a wave-atmospheric coupling, unlike the model used by ECMWF. Still, a short-term forecast of only a few hours ahead will probably be able to be more accurate if one or several wave buoys are located near-by the forecast area comparing the forecast with measurements and correct the forecast if necessary. [47]

Strategy 2 has been developed assuming that wave forecast on individual H_s measurements one to three hours ahead in time have a high accuracy. If the wind farm in figure 4.3 is built, the cost of making a wave model for the specific site is negligible compared to the huge cost of buying and installing the turbines, cables and other infrastructure. According to Yvonne Gusdal at DNMI[38], setting up a wave model should only take a couple of weeks before it can be used by the wind farm owner.

A control strategy combining measurements and forecast would have to be run from the SCADA (Supervisory Control And Data Acquisition) system, with the possibility of human intervention if large forecast or measurement malfunction should occur. Still, strategy 2 has been implemented and simulated assuming a fully automatic system.

Algorithm for control strategy 2

By running through each time step of H_s, it was assumed that future data points were forecasts and past data point were measurements. The forecast data was simply made by adding a random number between -0.25 and +0.75 m to H_s, which gives an average bias of +0.25 m according to equation 3.14 and is about the average through the year according to figure 3.14. The root mean square error (RMSE) for the forecast was calculated to be 0.382 using equation 3.15. This is low compared to the RMSE in figure 3.14, but this can be accepted if one assumes that the enhancement of the wave model in 2011 reduces the RMSE in winter and that the wave forecast model is improved further in general. Due to uncertainty in the forecast, a safety limit was also implemented in the $H_{s,cut\text{-}out}$ to always keep the system on the safe side.

Compared to strategy 1, the criteria for turning on and off the survival mode system is more complicated. When the turbine was in operation, the turbine would reconfigure into survival mode if one of the two criteria was fulfilled:

1. If $H_{s,measurement} > H_{s,cut-out}$ *or*
2. If $H_{s,forecast} > H_{s,cut-out} -$ safety limit

The time window of the forecast was set equal to *twice* the reconfiguration time; 2 ×20 min = 40 min for strategy 2a), 2 ×40 min = 80 min for strategy 2b) and 2 ×60 min = 120 min for strategy 2b). This would make sure that the turbine was in survival mode before the high waves arrive and at the same time avoid that the survival mode system did not turn on and off faster than the reconfiguration time allowed.

When the turbine was in survival mode, the control strategy would use a forecast of three hours ahead in time and not reconfigure back to operational mode before the forecast indicated that wave height would stay low for a while; this also avoids unnecessary reconfiguration into and out of survival mode. When in survival mode, both of the following criteria had to be fulfilled in order for the turbine to reconfigure back to operational mode:

1. If $H_{s,measurement} < H_{s,cut-out}$ *and*
2. If $H_{s,forecast} < H_{s,cut-out}$ − safety limit

If strategy 2 is simulated using $H_{s,cut\text{-}out} = 7.0$ m, safety limit = 0.5 m, reconfiguration time = 20 minutes (strategy 2a) and forecast window = 40 minutes, it would operate in the following way:

Turbine in operational mode:
if $H_{s,measurement} > 7.0$ m *or* $H_{s,+40\text{ min}} > (7.0\text{ m} - 0.5\text{ m})$
⇒ Shut down turbine and reconfigure into survival mode

Turbine in survival mode:
if $H_{s,measurement} < 7.0$ m *and* $(H_{s,+20\text{ min}}, H_{s,+40\text{ min}}, ..., H_{s,+3\text{ hours}}) < (7.0\text{ m} - 0.5\text{ m})$
⇒ Reconfigure into operational mode and re-start turbine

The calculation of energy loss was performed by removing all the energy production when the turbine was in survival mode and using the same delay as in strategy 1 to account for different reconfiguration times when the turbine goes back into operation. An illustration on how control strategy 2 would operate in the example time series of $H_s(t)$ from Draugen is shown in figure 4.11.

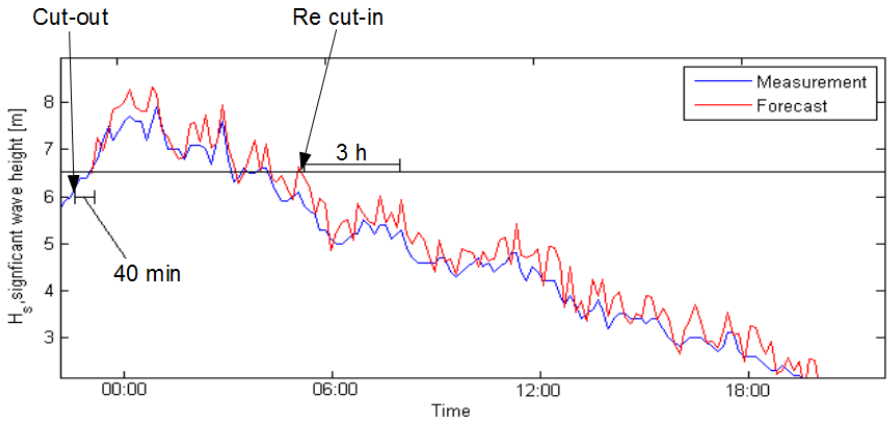

Figure 4.11: *Strategy 2a) with* $H_{s,cut-out} = 7$ *m, safety limit = 0.5 m, reconfiguration time = 20 minutes and forecast window = 40 minutes*

As it can be seen in the figure, the safety limit of 0.5 m does nothing else than to lower the $H_{s,cut\text{-}out}$ to 6.5 m and makes sure the turbine does not experience wave heights above its

limit. Strategy 2 seems to be a quite safe and efficient method that could potentially fulfil all three criteria significantly better than strategy 1. On the downside, the control strategy relies on high accuracy in the forecasting of waves to work properly. An accurate wave model must therefore be in place before such a system can be trusted blindly and there must anyhow be a safe mechanism that overrides the forecast if a measurement exceeds the $H_{s,cut\text{-}out}$.

4.3.4 Strategy 3 - Perfect forecast

A last control strategy named strategy 3 was simulated using the same algorithm as strategy 2, but assuming that a perfect forecast is available and that there is no safety limit. This is based on the idea that wave forecasting models may improve in the future and that a combined measurement-forecast system is developed where the forecast is continuously cross-checked against measurements. This might require human operation from the SCADA center, but as the experience with this kind of system increases through the life time of the project, the wind farm operation can be optimized further. Strategy 3 is simulated just to see how close one can possible get to the ideal energy loss without exceeding wave height limits of the turbine. Only the fastest reconfiguration time of 20 minutes is simulated using strategy 3. An illustration on how this strategy would operate is shown in figure 4.12.

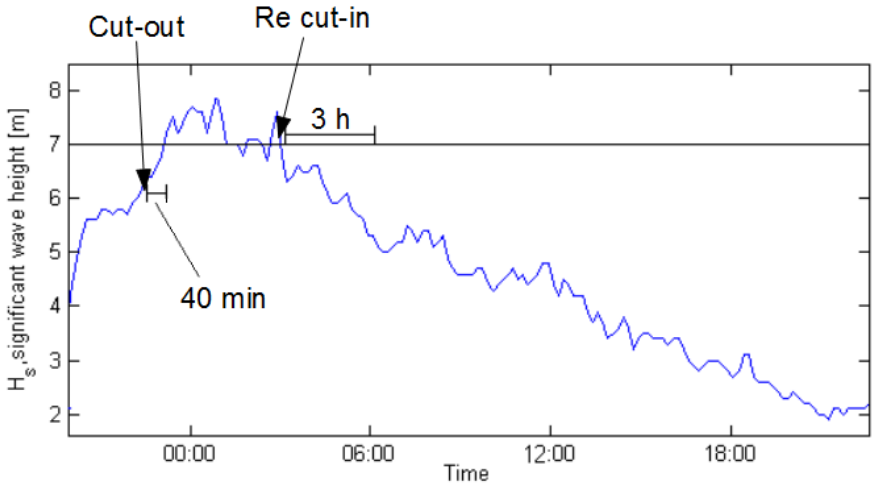

Figure 4.12: *Strategy 3 assuming perfect forecast and* $H_{s,cut-out} = 7$ *m, safety limit = 0.0 m, reconfiguration time = 20 minutes and forecast window = 40 minutes*

4.3.5 Other control systems

Although three control strategies using measurements and forecasting are presented here, there might be other control systems that could be implemented in the TLB B wind farm. One possibility is to measure loads directly on different components of the turbine, like the mooring lines or anchors. If, for any reason, measured loads on one of the components exceed a given threshold, the turbine shuts down and will not re-start before the measurements show a load decrease. The system could thereby protect the turbines from other damaging effects in

addition to high waves, such as a misalignment between wind and waves causing high loads. Still, the cost of implementing such as system and the uncertainty of having measurement equipment on every turbine could be problematic due to malfunction on the sensors.

Another possibility is to have a warning system around the wind farm consisting of wave buoys measuring H_s before they reach the turbines. This would require wave buoys to be placed in a ring around the wind farm to register waves coming from different directions. The distance from the wave buoys would be an issue, since they must be placed a certain distance away from the turbines so they are able to "warn" the wind farm before the waves hit. If one assumes that the reconfiguration time is 20 minutes and the average period of the waves is 10 seconds, it is possible to calculate the minimum distance between the wind farm and wave buoys by using equation 3.3, 3.4 and 3.6.

This distance was calculated to be around 10 km and would increase assuming longer reconfiguration times and wave periods. 10 km was considered to be a too large distance, since the wave height could change significantly before reaching the wind farm. There are also other arguments against a warning system like this with regards to cost of hiring more land and maintaining perhaps 50 - 100 wave buoys. None of these systems were looked into further.

4.4 Load simulations in 3Dfloat

It was now time to see how beneficial it might be to reconfigure into survival mode for the TLB B. The expectation was that the loads on different components of the turbine could be significantly reduced when moving the mooring lines to the root of the nacelle at high waves. This load reduction is necessary to achieve if there should be any point of loosing energy production from the wind farm. Furthermore, the idea is to be able to reduce the size of one of several components of the turbine (for instance the floater), which would mean a cheaper turbine in total.

Load simulations were carried out by Ph.D Anders Myhr in 3Dfloat, which is an *"aero-hydro-servo-elastic simulation tool developed from 2006 at IFE and UMB for the computation of dynamic response of offshore wind turbines"*[4]. Before the simulations could be performed, different load cases had to be defined. This was done in discussion with Anders Myhr and Tor Anders Nygaard and three load cases was to be simulated:

1. With the TLB B optimized for mooring lines in normal mode, the response in various components is simulated when the turbine is exerted to different wave heights up to extreme waves ($H_{s,50}$). The turbine is optimized in a way that the excess buoyancy determined by the size of the floater makes sure that the mooring lines are always taut.

2. The same TLB B, but with the mooring lines in survival mode, is simulated with the same waves as in case 1. If the force amplitudes in the mooring lines are lower compared to 1), there is less need for excess buoyancy and the size of the floater can be reduced.

3. With the TLB B optimized for survival mode (less mass in the floater), the turbine is exerted to extreme waves ($H_{s,50}$) in survival mode. A simulation is also run with the mooring lines in normal mode, but the maximum wave that hits the turbine in this mode will be the $H_{s,cut\text{-}out}$.

To find $H_{s,50}$ for the different sites, the approach explained in 3.3.2 using a Gumbel distribution was first used. Communication with DNMI and Kenneth Johannessen Eik in Statoil revealed that the values found using data collected in this thesis were to high[48, 44]. The reason for this was perhaps caused by the fact that one should have data for at least a third of the return period one wishes to calculate (16 years of data for $H_{s,50}$, 33 years for $H_{s,100}$). Another reason could be that the data was not independent (there should be at least 48 hours between high wave heights). Lastly, the GEV and GP distributions are more common to use for calculating extreme wave heights in Norwegian waters than the Gumbel distribution.

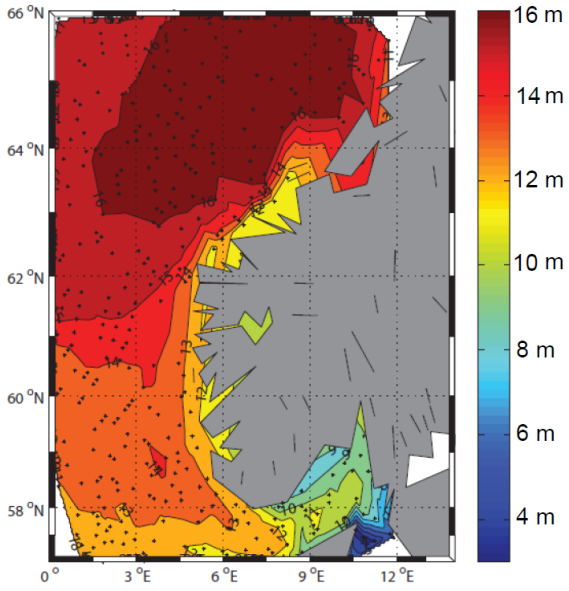

Figure 4.13: *Extreme significant wave height with a return period of 50 years in the North and Norwegian Sea*[48]

Performing these calculations was considered too time-consuming and instead, a map over $H_{s,50}$ in Norwegian waters was given by Kenneth Johannessen Eik, see figure 4.13. When using this data as input in 3Dfloat, it is important to remember the relationship between H_s and H_{max} given in equation 3.8. Therefore, exerting the TLB B to a $H_{s,50}$ wave = 16 m in 3Dfloat actually means sending a wave with a height of around 30 metres on the turbine!

4.5 Scaling data to fit potential floating turbine markets

As mentioned before, the wave climate in the North and Norwegian Sea is rough, at least compared to other places where there is a potential market for floating wind turbines in the

future. Sites that can be seen as a floating wind turbine market should fulfil certain criteria, such as a certain sea depth (< 50 m), nearness to demand centres and a relatively mild wave climate. This can be found in places like for example the east coast of the United States, the west coast of Japan and parts of the Chinese Sea.

To find $H_{s,cut\text{-}out}$ for other places, the same procedure explained in this chapter could have been followed using data from the specific site. Unfortunately, it was difficult to obtain meteorological data from other countries for free. One possibility was therefore to scale the available data by using the mean values, see section 3.3.1. For example, if one wishes to investigate the energy loss for different $H_{s,cut\text{-}out}$ at the east coast of United States by using data from the Heidrun platform, one multiplies all the wave height data with a constant equal to the relationship between the mean significant wave height at the different places:

$$H_{s,US} = \frac{\bar{H}_{s,US}}{\bar{H}_{s,Heidrun}} \cdot H_{s,Heidrun} \tag{4.2}$$

This has been done using data from Heidrun assuming that the wind speed conditions are the same and downscaling the wave height data to fit several places. The mean significant wave height data are gathered from the map in figure 3.8 and the ideal energy loss at different $H_{s,cut\text{-}out}$ and an optimal $H_{s,cut\text{-}out}$ was found.

It must be emphasized that this method is highly uncertain, firstly because one assumes that the wave height distribution is maintained only shifting it linearly to the left without considering any differences in the Weibull shape parameter[47]. Additionally, due to different weather systems and phenomenons like hurricanes or typhoons, a lower value of $H_{s,mean}$ does not necessarily mean a lower value of $H_{s,50}$. There is also a limit on how low the optimal $H_{s,cut\text{-}out}$ might be, since there could be other things than extreme waves that will dimension the turbine (e.g transportation, installation)[49]. Despite of all this, simulations with wave heights using equation 4.2 for different places have been done to investigate what would be the impact on the $H_{s,cut\text{-}out}$ using a lower mean significant wave height.

Chapter 5

Results

In this chapter, the main results from the wind and wave data analysis and load simulations in 3Dfloat will be presented. To avoid overwhelming the reader with information, it has been attempted to show only the key part of the results here. A complete and more detailed version of the results can be found in the appendices.

The data from each site has been run through the same MATLAB script, only adapted to the site-specific parameters like the anemometer height and the reduction factor from table 4.1. The focus in the results has been on finding an optimal value for $H_{s,cut\text{-}out}$, besides investigating the differences in performance between the various strategies and reconfiguration times.

5.1 Ideal energy loss at different $H_{s,cut\text{-}out}$

The ideal energy loss (assuming negligible reconfiguration time) at different $H_{s,cut\text{-}out}$ for each site has been found and is plotted in figure 5.1:

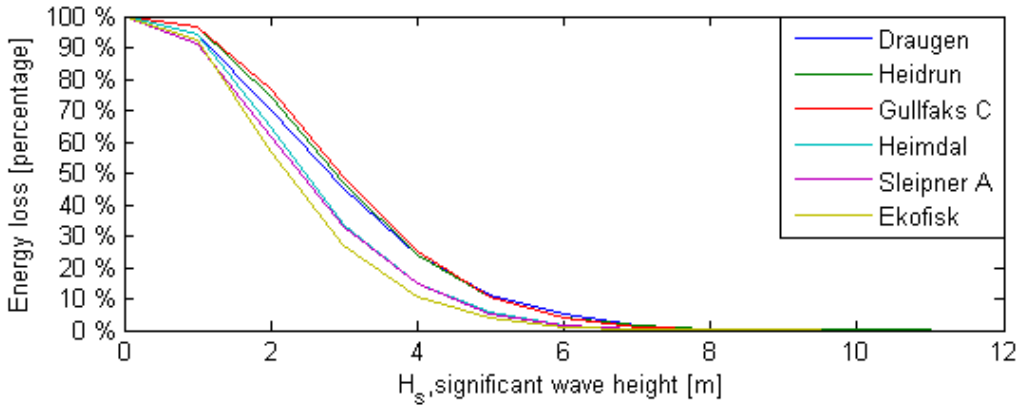

Figure 5.1: *Ideal energy loss at different $H_{s,cut\text{-}out}$, all sites*

The figure indicates that Ekofisk has the mildest wave climate and Draugen the roughest. Still, the curves seem to converge when approaching an ideal energy loss of under 1%, which has been defined as an acceptable limit.

In table 5.1 key data for each site is given, like the annual energy production without the cut-out wave height. The ideal energy loss has been calculated for two cases, namely a *low* and a *high* $H_{s,cut\text{-}out}$. These were both chosen as preliminary optimal $H_{s,cut\text{-}out}$ and used as

input when calculating the real energy loss using different strategies and reconfiguration times. As it can be seen in the table, the values for the $H_{s,cut\text{-}out}$ lie between 7 - 9 m for all the sites, which seems to be about 3 - 4 times the value of $H_{s,mean}$.

Table 5.1: *Key data from sites, including a low and high* $H_{s,cut\text{-}out}$

				$H_{s,cut\text{-}out}$ (Ideal energy loss)		
	$H_{s,mean}$	$H_{s,max}$	AEP	Low	High	$\frac{H_{s,cut-out}}{H_{s,mean}}$
Ekofisk	1.91 m	10.9 m	23.7 GWh	7 m (0.25%)	8 m (0.06%)	3.9
Sleipner A	2.16 m	11.3 m	27.1 GWh	7 m (0.27%)	8 m (0.04%)	3.5
Heimdal	2.19 m	10.0 m	26.2 GWh	7 m (0.42%)	8 m (0.10%)	3.4
Gullfaks C	2.66 m	12.8 m	26.7 GWh	7 m (1.02%)	8 m (0.20%)	2.8
Draugen	2.45 m	13.0 m	23.2 GWh	8 m (0.57%)	9 m (0.18%)	3.5
Heidrun	2.57 m	16.5 m	24.6 GWh	8 m (0.44%)	9 m (0.13%)	3.3

5.2 Results from sensitivity analysis

The sensitivity analysis was performed as described in section 4.2.6. The ideal energy loss at different cut-out wave heights for the base case using the NREL 5 MW-turbine was compared with four other cases; two of which the wind speed had been scaled up or down and the last two using power curves for other wind turbines. As the same trend was observed for all the sites, only one of them, Draugen, is shown here. The results for the other sites can be found in Appendix B.

It must be kept in mind that the ideal energy loss is calculated using the deviation from the annual energy production without the cut-out wave height. Since the AEP varies from case to case and due to different power ratings of the turbines, the full load hours is also calculated because this is an easier parameter to use when comparing the power output from the various cases,, see table 5.2.

Table 5.2: AEP and full load hours in the sensitivity analysis, Draugen

	AEP (GWh)					Full load hours (h)				
	NREL	u+10%	u-10%	E-126	V90	NREL	u+10%	u-10%	E-126	V90
Draugen	23.2	25.3	20.8	33.9	12.3	4642	5057	4164	4523	4087

The ideal energy loss for the various cases for the Draugen site is shown in figure 5.2. If the $H_{s,cut\text{-}out}$ = 8.0 m, one can observe the difference in energy loss for the various cases. It seems to be a very small deviation in energy loss using different turbine types. Scaling the wind speed will on the other hand have a larger impact; increasing the wind speed will lower the energy loss and vice versa. Still, the difference is minimal when raising the $H_{s,cut\text{-}out}$ to 9.0 m.

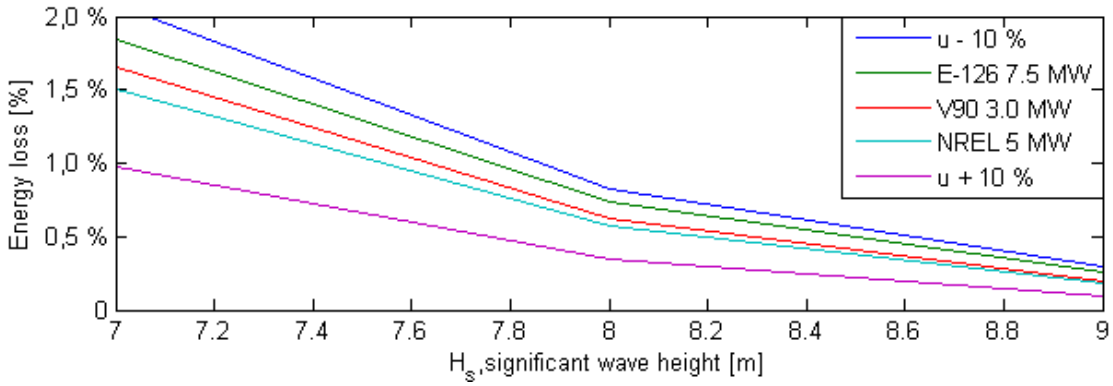

Figure 5.2: *Ideal energy loss for the different cases in the sensitivity analysis, Draugen*

5.3 Performance of control strategies

In section 4.3.1, three criteria to evaluate the various control strategies were defined; energy loss, experienced waves in normal configuration and number of reconfigurations. In this section, the difference in performance between the three strategies is presented in addition to investigating how the reconfiguration time affects the results.

Although the simulations have been run for both the low and high $H_{s,cut\text{-}out}$ defined in the previous section, the difference between the strategies was quite similar. Only the results from using the high $H_{s,cut\text{-}out}$ are presented here, but all results from the simulations of the control strategies using both values of $H_{s,cut\text{-}out}$ are given in Appendix C.

5.3.1 Energy loss

The energy loss for the different sites using strategy 1a), 2a) and 3) (reconfiguration time = 20 minutes) can be seen in figure 5.3. The energy loss for both strategy 1a) and 1b) are similar for all the sites, both having a value several times the ideal energy loss. Strategy 3), which assumes no safety limit and a perfect forecast, approaches the ideal value significantly more and is about twice the lowest achievable energy loss.

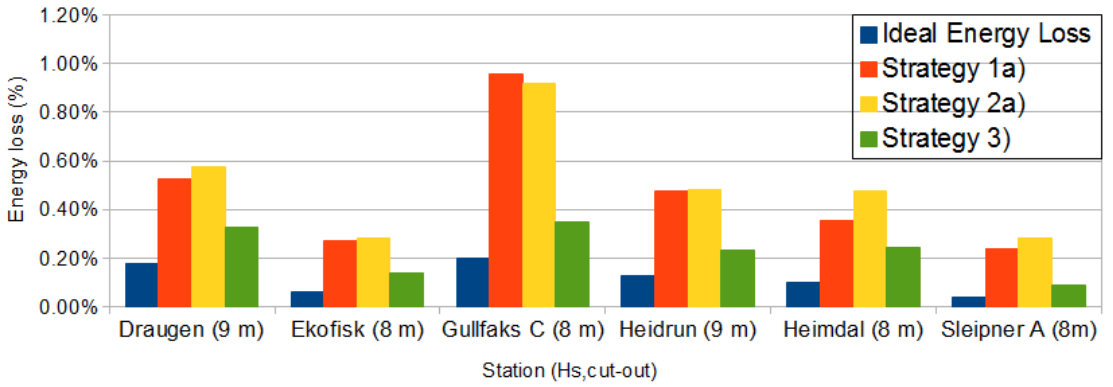

Figure 5.3: *Energy loss for all sites using different strategies. Reconfiguration time = 20 min*

It can also be observed that although the ideal energy loss for Draugen and Gullfaks is almost the same, the real energy loss using strategy 1 and 2 is significantly higher for Gullfaks. One reason for this could be that H_s exceeds $H_{s,cut\text{-}out}$ more frequently, but lasts a shorter amount of time at Gullfaks. This increases the number of annual reconfigurations (see figure 5.7), which has a negative impact on the energy loss. This illustrates that the characteristics of the wave climate (and not just $H_{s,mean}$) will have an impact of the difference between the ideal energy loss and the energy loss using various control strategies.

The difference in energy loss for strategy 1 (red bars) and strategy 2 (yellow bars) at Draugen assuming different reconfiguration times is shown in figure 5.4. This reveals that strategy 2 is more sensitive to the reconfiguration time than strategy 1, a trend observed in the other sites as well. The reason for this is that the reconfiguration time in strategy 1 only affects the energy loss by the difference in delay when the turbine re cuts-in after being in survival mode. In strategy 2 on the other hand, the reconfiguration time also have an influence on when the turbine cuts out (see figure 4.11), causing a larger difference in energy loss.

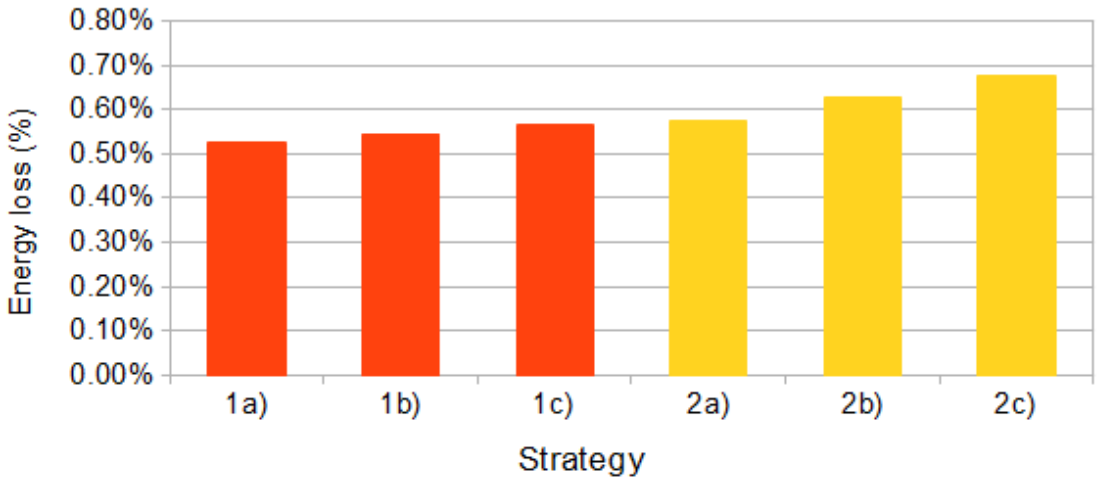

Figure 5.4: *Energy loss strategy 1 and 2 assuming different reconfiguration times (a) = 20 min, b) = 40 min and c) = 60 min), $H_{s,cut\text{-}out}$ = 9.0 m, Draugen*

5.3.2 Waves experienced by the turbine in normal configuration

Although it is important that a control strategy minimizes the energy loss, it is absolutely vital that it makes sure that the TLB B is in survival mode when high waves hit the turbine structure. If the turbine is exerted to higher waves in operational mode than what it is designed for, this could lead to damage on one or several turbine components or in the worst case, destroy the whole turbine. This adds to the cost of energy delivered by the wind farm and makes the wind power project less economically viable.

To investigate the performance of this criterion for the different strategies, the highest significant wave height experienced by the turbine in normal configuration (or during

reconfiguration) has been found for all strategies. This is shown for strategy 1a), 2a) and 3) in figure 5.5.

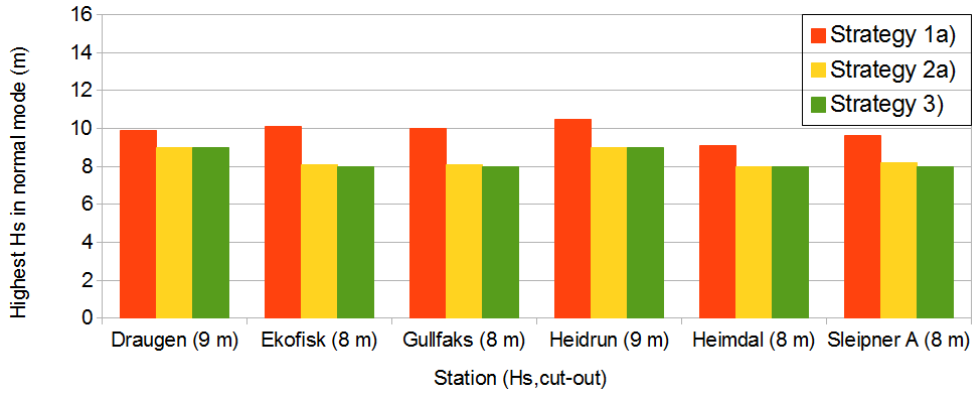

Figure 5.5: *Highest H_s experienced in normal mode using different strategies, all sites*

While the highest wave experienced by the TLB B using strategy 2a) and 3) is almost always equal to the $H_{s,cut\text{-}out}$, it seems strategy 1 does not manage to get the turbine in survival mode fast enough and the turbine experiences significant wave heights 1 - 2 metres above the $H_{s,cut\text{-}out}$. The reason for the poor performance of strategy 1a) is that although the turbine cuts out at the $H_{s,cut\text{-}out}$, it spends 20 minutes reconfiguring into the survival mode system. If the wave height increases rapidly in this period, the turbine will experience waves higher than the cut-out wave height before the reconfiguration is complete.

This phenomenon gets worse using strategy 1b) and 1c), where the reconfiguration time is even longer (40 and 60 minutes respectively), see figure 5.6. Strategy 2, on the other hand, is less insensitive to the reconfiguration time because of the use of forecasting, which makes sure the turbine rarely experiences $H_s > H_{s,cut-out}$.

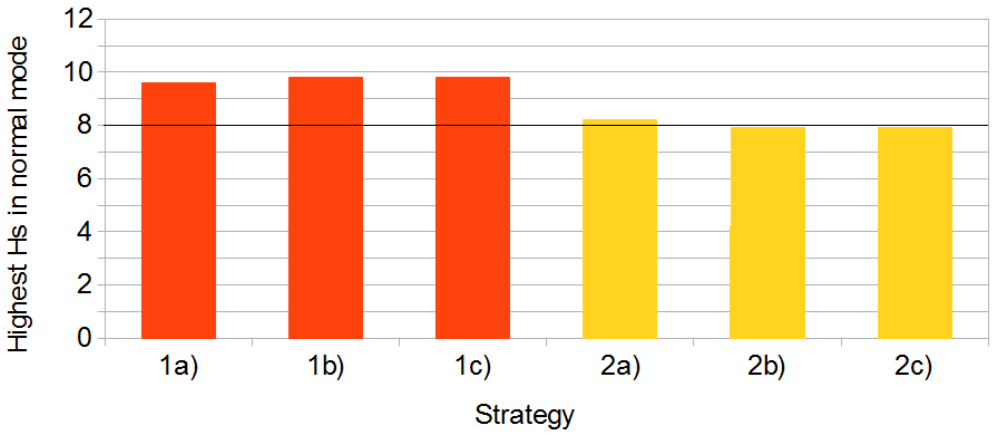

Figure 5.6: *Highest H_s experienced by the turbine using strategy 1 and 2 assuming different reconfiguration times, $H_{s,cut\text{-}out}$ = 8.0 m (black line), Sleipner A*

5.3.3 Number of reconfigurations

The different strategies are also tested against a last criterion; that the control strategy avoids that the survival mode system turns on and off rapidly when the wave height oscillates around the $H_{s,cut\text{-}out}$. This was measured by checking if the time between each cut-out and re cut-in was at least twice the time spent for reconfiguration; enough to switch the survival mode system on *and* off. While this criterion was always fulfilled by strategy 2 and 3, this problem could occur more often when using strategy 1 before the correct $H_{s,recut-in}$ was chosen. Preliminary results showed that this issue occurred when the difference between $H_{s,recut-in}$ and $H_{s,cut\text{-}out}$ was too small; this was the reason for choosing a $H_{s,recut-in} = H_{s,cut-out} - 2$ m (and not 1 m or 0.5 m).

In addition, it is possible to check if the survival mode system operates reasonably is measuring the number of annual reconfigurations into and out of survival mode, denoted $N_{reconfig}$. This indicates how many cycles the survival mode system experiences through the life time of the wind farm. If $N_{reconfig}$ exceeds a certain limit, this could lead to fatigue in the survival mode system, whose magnitude depends on which reconfiguration system is chosen for the TLB B. In figure 5.7 $N_{reconfig}$ is shown for the different strategies. In addition, the number of reconfigurations for the ideal situation (no reconfiguration time) belonging to the ideal energy loss is also presented.

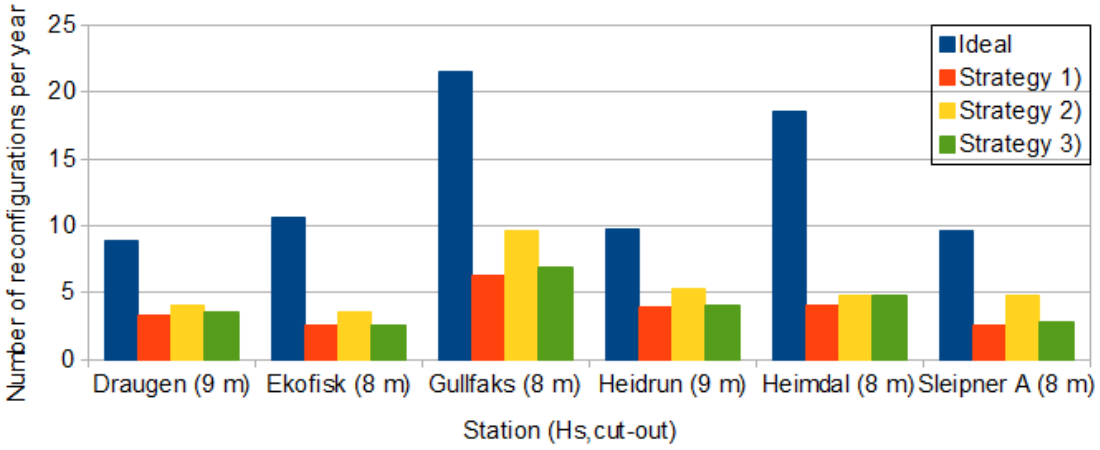

Figure 5.7: *Number of annual reconfigurations using different strategies*

It can be seen that $N_{reconfig,ideal}$, which is really a number for how often H_s crosses the cut-out wave height limit, has a significantly higher value than for the different strategies. This makes sense, since the strategies are designed not to turn on and off too often due to limitations with the reconfiguration time. There are small differences between the strategies, although strategy 2 has a significantly higher value of $N_{reconfig}$ for some sites. $N_{reconfig}$ is the same for the different reconfiguration times since this only controls *when* the turbine goes into survival mode and not how many times it will do so.

5.4 Results from the load simulations

The results from load case 1) and 2) basically showed that there was only a small difference in load response between the normal and survival mode configuration of the mooring lines. When the turbine was exerted to extreme waves ($H_{s,50}$) the force amplitudes on the lower mooring lines actually increased some for the survival mode (for details see figures D.1 - D.4, Appendix D). This indicated that the mass of the floater could not be reduced, since this would lead to slack mooring lines that in some cases which could probably lead the mooring lines to snap. The result made it very difficult to simulate load case 3), which should ideally have been performed using $H_{s,50}$ and $H_{s,cut\text{-}out}$ from all six sites to compare the steel mass reduction in the floater with the energy loss from introducing the survival mode.[50]

A last minute effort was made to try to get some valid results from the load simulations in 3Dfloat. New simulations were performed by Anders Myhr after making some adjustments, like *"increasing the mooring line radius from 120 metres to 200 metres to better illustrate the difference in response between normal and survival mode, which also makes it easier to adjust the eigenperiods manually"*[51]. Extreme wave and calm sea simulations were run on the same turbine structure (with the same excess buoyancy) with the top mooring lines in three different positions (position indicated as metres above water level):

1. 22.5 m (Standard/Normal mode)
2. 54.0 m (Survival mode)
3. 84.0 m (Survival05 mode)

The positions of the mooring lines in Standard and Survival mode were the same as tested in the earlier load cases, while the position of Survival05 mode was found through trial and error[51]. The load amplitudes for the top and bottom mooring lines in addition to the anchor load for Survival and Survival05 mode was then compared to the same load amplitudes simulated in Standard mode, see table 5.3.

Table 5.3: *Relative load amplitudes at mooring lines and anchors for the three different positioning of mooring lines (At calm sea the maximum loads (and not amplitudes) has been compared) [51]*

	Components	Standard	Survival05	Survival
Extreme wave	Top lines	100%	50%	28%
	Bottom lines	100%	97%	122%
	Anchors	100%	91%	81%
Calm sea	Top lines	100%	93%	80%
	Bottom lines	100%	100%	87%
	Anchors	100%	90%	80%

When moving the upper mooring lines upwards, more of the loads are transferred to the bottom lines and the loads on the bottom lines are actually larger for Survival mode than Standard mode at extreme waves. Survival05 mode is able to achieve a general decrease in loads and there seems to be a linear decrease in anchor loads as the mooring lines are moved upwards. Still, the main advantage of the Standard mode is that since it does not move the mooring lines at all, the load amplitudes are nearly constant, a desired property when dimensioning the mooring lines[51]. It is emphasized that the results are sensitive to some details like for instance the wave period, but the trend of these results is clear[51]. The detailed results from these simulations are given in Appendix D.

5.5 Consequences of wave data scaling

The scaling of the wave data from Heidrun has been used to investigate what could the optimal $H_{s,cut\text{-}out}$ in other wave climates than in the North and Norwegian Sea. The mean significant wave height at Heidrun in the measurement period is $\bar{H}_{s,Heidrun} = 2.57$ m. By first scaling the H_s data linearly with a factor such that $\bar{H}_{s,Heidrun} = 2.25$ m, 2.00 m, ..., 1.00 m and running simulations, the ideal energy loss has been calculated for different values of $H_{s,cut\text{-}out}$, which is plotted in figure 5.8.

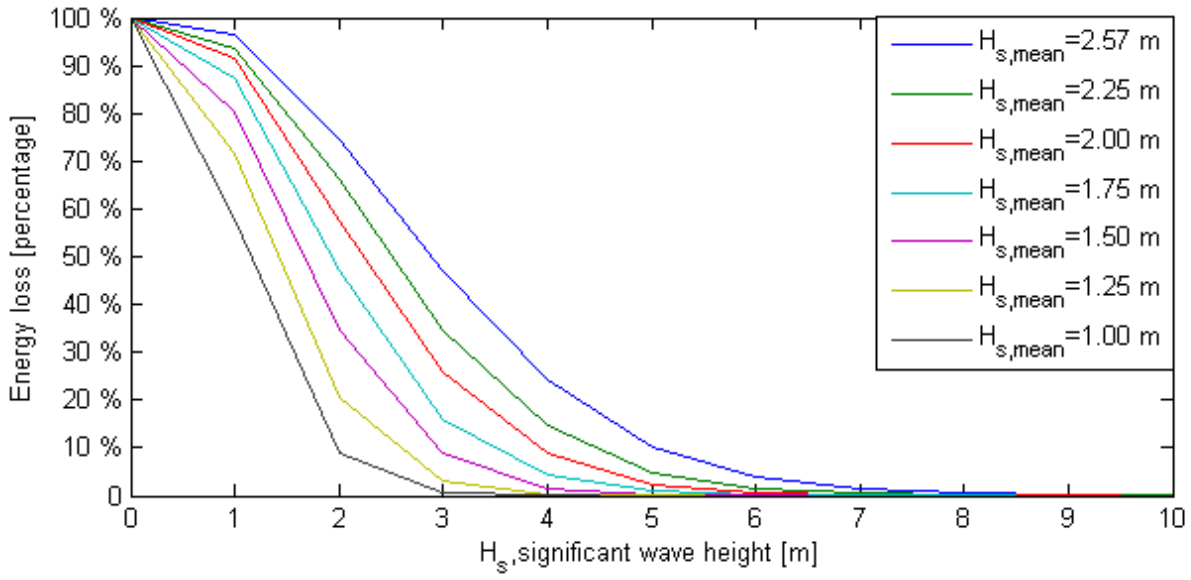

Figure 5.8: *Ideal energy loss at different $H_{s,cut\text{-}out}$ by scaling of Heidrun wave data*

The figure shows that the ideal energy loss curve is shifted to left as the value of $H_{s,mean}$ decreases, thus lowering the optimal $H_{s,cut\text{-}out}$. In table 5.4 each $H_{s,mean}$ has been linked up to a location where there might be a potential for a floating turbine market in the future using the map in figure 3.8. Results show that for each reduction in $H_{s,mean}$ of 0.25 metres, the

optimal $H_{s,cut\text{-}out}$ is lowered with 1.0 meter. This result follows the same trend as in table 5.1, which is that the optimal $H_{s,cut\text{-}out}$ seems to be about 3 - 4 times the value of $H_{s,mean}$.

Table 5.4: Optimal $H_{s,cut\text{-}out}$ for different locations using scaling of Heidrun wave data [32]

Location	$H_{s,mean}$	Reduction factor	$H_{s,cut\text{-}out}$ (Ideal energy loss)	$\frac{H_{s,cut-out}}{H_{s,mean}}$
Heidrun	2.57 m	1.0	9 m (0.13%)	3.5
California, USA	$\simeq$ 2.25 m	0.875	8 m (0.10%)	3.6
Maine, USA	$\simeq$ 2.00 m	0.778	7 m (0.13%)	3.5
China (east coast)	$\simeq$ 1.75 m	0.681	6 m (0.15%)	3.4
Japan (west coast)	$\simeq$ 1.50 m	0.583	5 m (0.22%)	3.3
India (west coast)	$\simeq$ 1.25 m	0.486	4 m (0.31%)	3.2
Australia (north coast)	$\simeq$ 1.00 m	0.389	3 m (0.58%)	3.0

Chapter 6

Discussion

There are many aspects to discuss in this master's thesis, both regarding the method and the results. While some issues have already been discussed previously, this chapter will focus on the most important parts of the approach and the main findings.

6.1 Quality assessment of materials and method

As it can be seen in three first blocks of the method flow diagram (figure 4.1), all the meteorological data sets from the various sites have been processed through several steps in order to find the optimal $H_{s,cut\text{-}out}$ with its belonging ideal energy loss and investigate the performance of the different strategies. Due to this linear data processing, any systematic or random error in the raw data or in one of the processing steps propagates into the simulations and might lead to errors or uncertainties in the results. Since the impact of each error will vary, it is important to identify which factors that could have led to significant uncertainties in the calculations.

6.1.1 Factors influencing the ideal energy loss and optimal $H_{s,cut\text{-}out}$

Although the meteorological data sets has gone through a quality control by the DNMI, the data may contain systematic errors. One example is that wind anemometers are disturbed by nearby obstacles, which may have led to both lower (wake effect) and higher (tunnelling effect) wind speeds[47]. While the degree of systematic error in the measurements is unknown, the amount of missing data and the quality of the data available has been assessed (see table 4.2). This showed that the data quality is satisfactory or better for all sites except Sleipner A, but this station has the advantage that many years of data is available. The error caused by the interpolation of missing data is in general considered negligible. Still, there is a chance that the measurements from stations with few years of available data (e.g. Draugen) are not entirely representative for the specific site.

While the shear exponent is set to $\alpha = 0.1$ when scaling the wind speed to hub height (90 m), this value will in reality vary depending on factors like atmospheric stability and temperature. The uncertainty from the assumption that α is constant is greater for sites where there is a large difference between the measurement height $Z_{anemometer}$ and the hub height Z_{hub} (e.g. Gullfaks C, difference = 53 m). Another source of error is the assumption that the 10-minute mean wind speed in hub height u_{hub} equals the mean wind speed in the rotor area and that

u_{hub} is constant within the measurement interval (20 minutes). The total uncertainty of u_{hub} due to these assumptions could be significant.

To deal with the uncertainties having an impact on especially u_{hub} and consequently the energy production calculations, two measures were taken. The first was the comparison of the mean wind speed and annual energy production with the Enova report[45], which is shown in table 4.3. The comparison showed good agreement between the Enova report and the thesis, although deviations were found for Draugen and Ekofisk. This is probably because too few years of data have been gathered or that the data sets are from different time periods. To investigate how much these deviations and other factors like the choice of power curve could affect the choice of the optimal $H_{s,cut\text{-}out}$, the sensitivity analysis was performed.

This showed that neither scaling up or down the wind speed nor using power curves from other turbines had any significant impact on the choice of the $H_{s,cut\text{-}out}$, even though these factors affect the value AEP and full load hours. This indicates that the quality of the meteorological data sets and the processing of these to calculate the ideal energy loss at different $H_{s,cut\text{-}out}$ is acceptable for the applications used in this thesis.

6.1.2 Control strategy assumptions

Three different control strategies for the survival mode system were designed and simulated, with strategy 3 being a special case of strategy 2 assuming perfect forecast. Other designs were also looked upon during the working process, but the chosen control strategies were developed focusing on a simple design and that the survival mode system should have few criteria for when it turns on and off. It could be argued that strategy 1 should have been designed with a safety limit (as done for strategy 2) to reduce the chance of wave with heights exceeding the $H_{s,cut\text{-}out}$ will hit the turbine structure in operational mode. Still, this would make the survival mode system turn on and off too often, which can only be avoided by lowering the $H_{s,re\ cut-in}$; both changes leading to higher energy losses.

The wave forecasting error used in strategy 2 was based on the information provided by DNMI[35]. Since the calculation of the RMSE in the wave forecast simulated in strategy 2 was lower than that calculated in [35] (see figure 3.14), one can argue that the wave forecasting in reality is not this accurate. Furthermore, the bias and RMSE are only parameters that give averaged values of the deviation between forecasts and measurements, meaning that individual forecasts may be more erroneous than that which has been simulated in strategy 2.

According to Kjeller Vindteknikk[47], there might be events where the wave model erroneously forecasts individual wave heights 1 - 2 metres below the actual H_s, which could potentially be very harmful to the wind turbine. Before constructing a TLB B wind farm at a given site, a good understanding of the weather systems that can cause the wave height to increase rapidly in this area is needed. The phenomenon emphasizes that the accuracy of the wave forecasting should be high and that the reconfiguration into the survival mode system

should take a shorter amount of time than these fast changes in H_s. The assumption of a perfect forecast used in strategy 3 will never be a reality, although a wave forecasting model adapted for a specific wind farm site running from the SCADA center might come close.

6.2 Interpretation of main results

6.2.1 Energy loss and the choice of $H_{s,cut\text{-}out}$

The ideal energy loss (see figure 5.1) reveals significant differences between the sites for low values of $H_{s,cut\text{-}out}$. This reflects the various wave climates at the measurement stations and indicates that the wave height is higher in the Norwegian Sea (Draugen and Heidrun) and northern part of the North Sea (Gullfaks C). Still, if the acceptable limit of energy loss is roughly 1% of the AEP, the optimal $H_{s,cut\text{-}out}$ for all the sites is at least 8 metres, which is where the ideal energy loss curves start converging towards zero.

From the simulation results of strategy 1, 2 and 3, it became clear that the real energy loss assuming a strategy and a realistic reconfiguration time was considerably higher than the ideal energy loss, see figure 5.3. The high value of $H_{s,cut\text{-}out}$ from table 5.1 had to be chosen for all the sites to avoid an energy loss of more than 1%. It is implied that $H_{s,cut\text{-}out}$ seem to lie about 3 - 4 times the value of $H_{s,mean}$ for all the sites and that this may be made as a rule of thumb. Still, this is not an exact science and the hypothesis may only be valid for this oceanic region.

The definition of the optimal $H_{s,cut\text{-}out}$ changed after few positive results could be extracted from the load simulations in 3Dfloat. Originally, the real energy loss was to be compared with the load and/or cost reduction of an optimized TLB B structure at different cut-out wave heights, in which the optimal $H_{s,cut\text{-}out}$ would be the point where the gain was maximum. This would have answered if an acceptable energy loss for the wind farm should be 0.1%, 1% or even 10%. As the challenges with survival mode system has not been entirely solved within the time frame of this thesis, a qualified guess has been done to determine the optimal $H_{s,cut\text{-}out}$ assuming that the acceptable energy loss is less than 1%. The value of the optimal cut-out wave height was therefore chosen to be the high alternative (8 or 9 metres), taken from table 5.1.

6.2.2 Differences between strategies

Strategy 3 contains the unrealistic assumption that a perfect forecast is available, which is the reason why it performs better than the other strategies based on the three criteria. Comparing the first two strategies is therefore more interesting. The operation of strategy 1 and 2 is substantially different, the first only using measurements and the second combining measurements and forecasting. Both strategies have similar performance regarding the energy loss and the number of reconfigurations for all the sites (see figure 5.3 and 5.7), although strategy 2 is more sensitive to the reconfiguration time than strategy 1 regarding these criteria.

The control strategies differ more significantly in the criterion measured by the waves experienced by the turbine in normal reconfiguration. Since strategy 1 only operates according to measurements and is unable to predict future wave heights, the turbine will in many cases experience wave heights exceeding the cut-out wave height in normal configuration or during reconfiguration into survival mode. These events are especially severe when the wave height increases with several metres during a short period of time.

Figure 5.5 indicates that if strategy 1 is chosen for the TLB B, a turbine that cuts out at $H_s = 9.0$ m will have to be designed to endure a $H_s \simeq 11$ m. This greatly reduces the potential to minimize the steel mass in the floater which implies that only a small gain is obtained from introducing the survival mode system in terms of cost reduction. Strategy 1 is also more sensitive to the reconfiguration time than strategy 2 (see figure 5.6) regarding this criterion. This calls for a fast survival mode system if strategy 1 is to be implemented.

To sum up, strategy 2 (and 3) is preferred over strategy 1 due to the advantages that the forecasting gives, especially in terms of how the strategy is able to turn on the survival mode system in time, before high waves arrive. A strategy using forecast is therefore much safer than strategy 1, a vital factor considering the total cost of damage to a wind turbine or the whole wind farm. The catch of strategy 2 is that it requires a high accuracy of the wave forecasting, which must be in order before this control strategy is chosen. Nevertheless, the cost of making site-specific wave models able to predict H_s accurately is negligible compared to the total investment of the wind farm and the control strategy will anyhow have a safe system if forecasts should fail. The only way that strategy 1 could be a relevant alternative to strategies using forecasts, is by developing a fast survival mode system with a reconfiguration time of only a few minutes. Still, it is unknown how achievable this is.

6.2.3 Issues regarding load simulations

Load case 3) could still have been tested in 3Dfloat using several, smaller floaters in the TLB B and finding an optimal floater size by iteration, but the results from load case 1 and 2) indicated that none of these smaller structures could have survived a $H_{s,50}$-wave. This does not necessarily mean that the survival mode system in general is a bad idea, but that there are still several challenges left to solve with the reconfiguration of the mooring lines. Due to the time limitations of this thesis, these challenges have not been dealt with yet.

Still, the last minute simulations that were run with the upper mooring lines in three different positions attempted to solve some of the problems. Introducing the survival mode will increase the variation in load amplitude and require stronger and thicker mooring lines (with higher stiffness), but will on the other hand decrease the loads on the anchors. This result indicates that more expensive mooring lines could reduce the cost of the anchors. Still, calculating if this is beneficial calls for a more detailed analysis which has not been performed in this thesis. Another aspect is that Survival05 mode performs better overall than the Survival mode and gives a moderate load reduction on all components. This implies that the

optimal position of the upper mooring lines in survival mode is lower than previously expected. It could also mean that the distance between the top and bottom mooring lines should in general (also for Standard mode) be greater.[51].

As the TLB B is an on-going project, figuring out how to make a properly working survival mode system will have to be investigated in the future. The TLB research group might come to a conclusion that the reconfiguration of mooring lines is not the best survival mode system at all, and that other solutions will work better and should be implemented instead (e.g ballasting the floater). The results in this thesis are still valid for all survival mode systems, since the energy loss at a given $H_{s,cut\text{-}out}$ and control strategy only depends on the reconfiguration time, which will be roughly the same no matter which system is chosen.

6.2.4 Wave data scaling implications

As it has been emphasized in section 4.5, the scaling approach is highly uncertain due to several reasons and one should not over-interpret the meaning of these results. Still, the scaling of the wave height data show qualitatively that the optimal $H_{s,cut\text{-}out}$ can be reduced in places with lower mean wave heights, which opens up the possibility to design several versions of the turbine adapted for different wave climates. This opportunity might give the TLB B floating turbine concept a great competitive advantage in what could be a huge market for floating wind power in the future. Although the scaling results imply that a turbine can be optimized for a $H_{s,cut\text{-}out}$ down to 3.0 m, there might be a minimum boundary for the cut-out wave height due to other dimensioning loads experienced during installation or transportation. To investigate this idea further, real meteorological data from various floating wind power markets should be gathered and simulated using the procedure described in this thesis.

Chapter 7

Conclusions and recommendations

Through the data processing of the meteorological wind and wave data from measurement stations in the North and Norwegian Sea, the ideal energy loss for the various sites at different cut-out wave heights has been calculated. When the acceptable limit of energy loss was set to 1%, the optimal $H_{s,cut\text{-}out}$ was found to be 8 or 9 metres. Various uncertainties in the energy production calculations had little effect on the choice of the $H_{s,cut\text{-}out}$. The scaling of the wave data to fit potential floating wind turbine markets indicated qualitatively that $H_{s,cut\text{-}out}$ will decrease linearly with a reduction of the mean significant wave height, but this result is uncertain since no real wave and wind data from other places have been used.

After developing and simulating different control strategies for the survival mode system, it became clear that the strategies combining measurements with forecast (strategy 2 and 3) are preferred over strategy 1, which only uses measurements as input. This is mainly due to the fact that strategies using forecasting are able to reconfigure the turbine into survival mode before the high waves arrive. Still, this is based on the assumption that there is always a high accuracy in the wave forecasting, which is not necessarily the case. The real energy loss for strategy 3 implies that it is possible to come near the ideal energy loss if a perfect forecast is available, even if the reconfiguration into survival mode takes some time. In general, the forecast model predicting wave heights is a vital factor for the TLB B wind turbine both with regards to energy loss and safety; much effort should therefore be made to make the model as accurate as possible.

The results from the load simulations in 3Dfloat does not imply that the survival mode system using reconfiguration of mooring lines is capable of reducing the mass of the floater. Still, the last minute simulations revealed that a moderate overall load reduction on the mooring lines and anchors could be achieved if the position of the upper mooring lines in survival mode is lowered, but this does not confirm that the mass of the turbine structure can be reduced. More work needs to be done to investigate if a significant load reduction can be achieved by the reconfiguration of mooring lines at extreme wave conditions.

In general, introducing the cut-out wave height and the survival mode system in the TLB B looks promising regarding energy loss, but issues regarding the load reduction and optimization of the turbine structure must be resolved before this can become a reality. Nevertheless, the TLB B as a low-cost floating wind turbine concept with the possibility of construction various versions adapted to different wave climates may give in an upper hand in the future floating wind power market.

7.1 Further work

This master's thesis has given many answers to which consequences there are for introducing the cut-out wave height for the TLB B, but there are still many improvements to be made or new aspects to investigate in the future. As the TLB B is an on-going project, there are many issues that may be looked into further by the research group itself or by master students within mechanics, energy physics and industrial economics.

As mentioned before, the accuracy of wave models is one subject which can be looked closer at, since this is an important factor for a control strategy using forecasting. It is especially interesting to examine events where wave models erroneously predicts individual wave heights several metres below the actual H_s and to find out how often and in which wave climates this could be a problem. To increase the understanding of the weather phenomenons that drive these rapid changes would be also an important contribution.

In order to find the optimal cut-out wave height for other climates, wind speed and wave height data from other geographical locations should be gathered and run through the same procedure as in this thesis. This could potentially confirm or weaken the results from the scaling of the wave data and give answer to whether various versions of TLB B should be designed or not, each adapted a specific wave climate.

More simulations in 3Dfloat must be run to figure out the problems with the reconfiguration of mooring lines. Additionally, wave tank experiments should be run to see if the survival mode system manages to reduce loads in real life and that an optimized structure withstand the design waves in normal and survival mode configuration. If this is solved, it would also be interesting to perform fatigue load analysis on the survival mode system in addition to the extreme load cases. These may show that the survival mode system reduces the fatigue load on the system as well.

Lastly, an thorough economic analysis of the survival mode system should be performed. This should include the gain from reducing mass in the floater and the reduced fatigue loads, and finally comparing this with the energy and income loss due to $H_{s,cut\text{-}out}$. It should be mentioned that an energy loss of 1% is not necessarily an income loss of 1%, since electricity prices may vary throughout the year. In the North and Norwegian Sea the wave climate is rougher in winter time which means that most of the energy loss is located in this season. In addition, the electricity prices in Norway are in average higher in winter; loosing 1% in AEP could actually mean loosing 3 - 4% in income. In other places, both the wave climate and the electricity price pattern throughout the year could be different, meaning that the energy loss will have individual economic consequences depending on the location where the wind farm is constructed. Taking these aspects into consideration when choosing the site-specific $H_{s,cut-out}$ would truly be an optimization of the cut-out wave height.

Bibliography

[1] PD Sclavounos, S. Lee, J. DiPietro, G. Potenza, P. Caramuscio, and G. De Michele. *Floating offshore wind turbines: tension leg platform and taught leg buoy concepts supporting 3-5 MW wind turbines.* European Wind Energy Conf. EWEC 2010, Warsaw, Poland, 20-23 April, 2010.

[2] European Wind Energy Association (EWEA). *The European offshore wind industry key 2012 trends and statistics.* 2013.

[3] Amy N Robertson and Jason Mark Jonkman. *Loads Analysis of Several Offshore Floating Wind Turbine Concepts.* National Renewable Energy Laboratory, US Department of Energy, Office of Energy Efficiency and Renewable Energy, 2011.

[4] A. Myhr and T.A. Nygaard. *Load Reductions and Optimizations on Tension-Leg-Buoy Offshore Wind Turbine Platforms.* 2012.

[5] A. Myhr, K.J Maus, and T.A. Nygaard. *Experimental and Computational Comparisons of the OC3-HYWIND and Tension-Leg-Buoy (TLB) Floating Wind Turbine Conceptual Designs.* 2011.

[6] Department of Energy and Climate Change (UK). Renewable Energy Roadmap, 2011.

[7] Scira Offshore Energy. *Sheringham Shoal. http://www.scira.co.uk/*, Accessed: 01/03/2013.

[8] Henrik Stiesdal (Chief Technology Officer Siemens Wind Power). *Hywind: The world's first floating MW-scale wind turbine.* Wind directions, Dec. 2009.

[9] Sustainablebusiness.com. *Maine Leads Trend Toward Floating Offshore Wind Turbine. http://www.sustainablebusiness.com/index.cfm/go/news.display/id/24556*, Accessed: 20/03/2013.

[10] American Bureau of Shipping. *Guide for building and classing floating offshore wind turbine installations.* 2013.

[11] Jason Mark Jonkman, S Butterfield, W Musial, and G Scott. *Definition of a 5-MW reference wind turbine for offshore system development.* National Renewable Energy Laboratory, 2009.

[12] M. de Prada Gil, O. Gomis-Bellmunt, A. Sumper, and J. Bergas-Jane. *Power generation efficiency analysis of offshore wind farms connected to a SLPC (single large power converter) operated with variable frequencies considering wake effects.* Energy (Elsevier), 2011.

[13] James F Manwell, Jon G McGowan, and Anthony L Rogers. *Wind energy explained: theory, design and application. 2nd edition.* John Wiley&Sons Ltd, UK, 2009.

[14] Enercon product overview. http://www.enercon.de/p/downloads/ENERCON_PU_en.pdf. Accessed: 21/03/2013.

[15] Vestas V90-3.0 MW brochure. http://www.vestas.com/Files/Filer/EN/Brochures/Vestas_-V_90-3MW-11-2009-EN.pdf. Accessed: 21/03/2013.

[16] Jarle Eek at Statkraft Offshore Wind Department. Personal communication by e-mail, March 2013.

[17] Enercon control system. http://www.enercon.de/en-en/754.htm. Accessed: 21/03/2013.

[18] Siemens High Wind Ride Through brochure. http://www.energy.siemens.com/hq/pool/hq/power-generation/renewables/wind-power/High_Wind_Ride_through_brochure.pdf. Accessed: 02/04/2013.

[19] Zekai Şen, Abdüsselam Altunkaynak, and Tarkan Erdik. *Wind Velocity Vertical Extrapolation by Extended Power Law.* Advances in Meteorology, 2012.

[20] S.T. Frandsen. *Turbulence and turbulence-generated structural loading in wind turbine clusters.* Risø National Laboratory, 2007.

[21] D. Swagata, K. Neeraj, and S. Surya. *Time-Domain Modeling of Tower Shadow and Wind Shear in Wind Turbines.* ISRN Renewable Energy, 2011.

[22] O. Ditlevsen. *Stochastic model for joint wave and wind loads on offshore structures.* Structural Safety(Elsevier), 2002.

[23] Det Norske Veritas. *Design of Offshore Wind Turbine Structures-Offshore Standard DNV-OS-J101.* 2011.

[24] NJ Tarp-Johansen. *Extrapolation including Wave Loads–Replacing the Distribution of Hs by a Suitable Percentile.* Recommendations for Design of Offshore Wind Turbines, Risø National Laboratory, Denmark, 2005.

[25] P. Agarwal and L. Manuel. *Simulation of offshore wind turbine response for long-term extreme load prediction.* Engineering Structures(Elsevier), 2009.

[26] Tor Anders Nygaard, Anders Myhr, and Karl J Maus. *A comparison of two conceptual designs for floating wind turbines.* 2009.

[27] E. Bouws, L. Draper, EDR Shearman, AK Laing, D. Feit, W. Mass, LI Eide, P. Francis, DJT Carter, and JA Battjes. *Guide to Wave analysis and forecasting. WMO-No. 702.* World Meteorological Organization, 1998.

[28] K. Torsethaugen and S. Haver. *Simplified double peak spectral model for ocean waves.* Proc. 14th Int. Offshore and Polar Eng. Conf., Toulon, France, 2004.

[29] S. Haver. *On the prediction of extreme wave crest heights.* Citeseer, 2004.

[30] M.D. Earle. *Nondirectional and directional wave data analysis procedures.* NDBC Tech. Doc, 1996.

[31] Statoil Internal. *Statfjord Late Life project, Metocean Design Basis.* Doc. no. 0044, 2003.

[32] Stephen Barstow Fugro OCEANOR AS. Personal communication by e-mail, March 2013.

[33] George Galanis, Peter C. Chu, George Kallos, Yu-Heng Kuo, and C.T.J. Dodson. *Wave height characteristics in the north Atlantic ocean: a new approach based on statistical and geometrical techniques.* Stochastic Environmental Research and Risk Assessment, 2012.

[34] Knut Iden at the Norwegian Meterological Institute. Personal communication by e-mail, february 2013.

[35] Yvonne Gusdal and Ana Carrasco. *Validation of the Operational Wave Models - Report 2011.* The Norwegian Meterological Institute, 2012.

[36] Yr.no - hav og kyst. http://www.yr.no/hav_og_kyst/. Accessed: 22/03/2013.

[37] Yr.no - wave forecast map for 58.99N 3.94Ø - Saturday 23th of march 02:00. http://www.yr.no/sted/Hav/58,99600_3,94022/b Accessed: 22/03/2013.

[38] Yvonne Gusdal at the Norwegian Meterological Institute. Personal communication by e-mail, March 2013.

[39] Sciencedaily.com. *Maximum Height of Extreme Waves Up Dramatically in Pacific Northwest.* http://www.sciencedaily.com/releases/2010/01/100125123233.htm, 2010 (Accessed: 18/03/13).

[40] Magnar Reistad. *Global warming can result in higher waves.* Cicerone 5/2001, 2001.

[41] I.R. Young, S. Zieger, and A.V. Babanin. *Global trends in wind speed and wave height.* Science (Volume 332, p. 451 - 455), 2011.

[42] eklima.no. *Gratis tilgang til Meteorologisk institutts vær- og klimadata fra historiske data til sanntidsobservasjoner.* Accessed: February - April 2013.

[43] Norsk Oljevernforening For Operatørselskap. *Regionalt planverk mot akutt forurensing.* http://planverk.nofo.no/webAP11.asp, Accessed: February 2013.

[44] Reidun Gangstø at the Norwegian Meterological Institute. Personal communication by e-mail, March 2013.

[45] J Sandgren, L Hjort, P Miranda, G Hamarsland, and K Ibenholt. *Potensialstudie av havenergi i Norge*. Made for ENOVA SF by Sweco Grøner in co-operation with ECON and Kjeller Vindteknikk, 2007.

[46] Anders Ågotnes and Catho Bjerkseter. Personal communication, April 2013.

[47] Erik Berge and Knut Harstveit at Kjeller Vindteknikk. Meeting at Kjeller, 3rd April 2013.

[48] Kenneth Johannessen Eik Statoil. Personal communication by e-mail, February 2013.

[49] Tor Anders Nygaard. Personal communication, Ås, March 2013.

[50] Load simulations of case 1) and 2) 3Dfloat performed by Anders Myhr. April 2013.

[51] Simulations in 3Dfloat performed by Anders Myhr. 9th May 2013.

Appendix A

Power curves

The power curves shown in figure 2.2 that is used for energy production calculations were gathered from different sources and is given in detail in table A.1.

Table A.1: *Power curves for NREL 5 MW, Vestas V90 and Enercon E-126 turbine [11, 15, 14]*

Wind speed	Power (kW)		
u_{hub} (m/s)	NREL 5 MW	Vestas V90	Enercon E-126
0	0	0	0
1	0	0	0
2	0	0	55
3	40.5	0	175
4	177.7	75	410
5	403.9	187	760
6	737.6	348	1250
7	1187.2	574	1900
8	1771.1	875	2700
9	2518.6	1257	3750
10	3448.4	1688	4850
11	4562.5	2118	5750
12	5000.0	2514	6500
13	5000.0	2817	7000
14	5000.0	2958	7350
15	5000.0	2994	7500
16	5000.0	3000	7580
17	5000.0	3000	7580
18	5000.0	3000	7580
19	5000.0	3000	7580
20	5000.0	3000	7580
21	5000.0	3000	7580
22	5000.0	3000	7580
23	5000.0	3000	7580
24	5000.0	3000	7580
25	5000.0	3000	6000
26	0	0	5000
27	0	0	4000
28	0	0	3000
29	0	0	2000
30	0	0	1000
31	0	0	0

Appendix B

Sensitivity analysis

The energy production calculations performed for the sensitivity analysis and the energy loss at different $H_{s,cut\text{-}out}$ for all the sites is shown in table B.1 and figure B.1.

Table B.1: *Annual energy production and full load hours in sensitivity analysis, all sites*

	AEP (GWh)					Full load hours (h)				
	NREL	u+10%	u-10%	E-126	V90	NREL	u+10%	u-10%	E-126	V90
Ekofisk	23.7	25.8	21.2	34.4	13.5	4733	5158	4231	4587	4497
Sleipner A	27.1	28.5	25.1	39.9	14.5	5417	5702	5020	5318	4835
Heimdal	26.2	27.8	24.1	38.5	14.0	5243	5559	4820	5133	4672
Gullfaks C	26.7	28.2	24.7	39.4	14.3	5340	5632	4950	5248	4754
Draugen	23.2	25.3	20.8	33.9	12.3	4642	5057	4164	4523	4087
Heidrun	24.6	26.4	22.4	36.2	13.1	4922	5278	4487	4821	4353

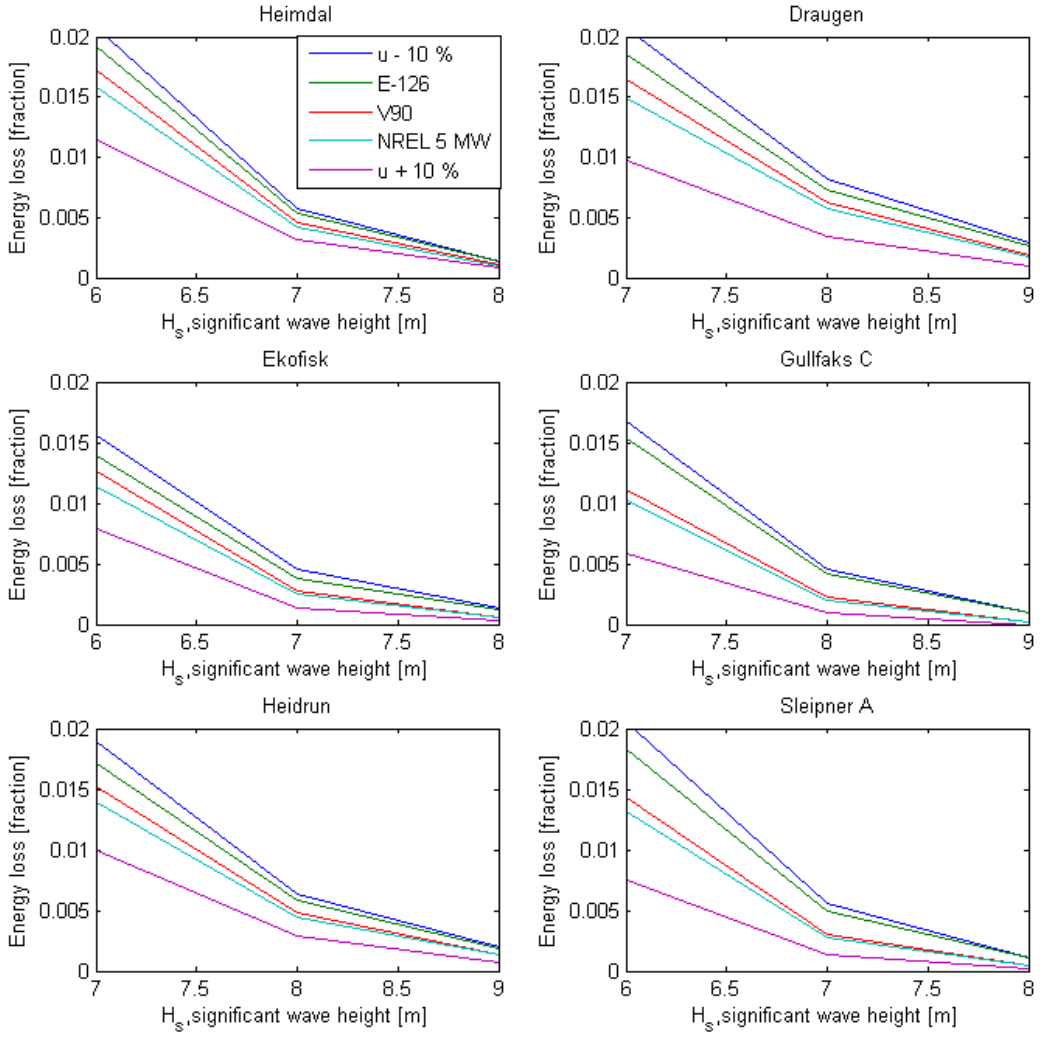

Figure B.1: *Ideal energy loss at different $H_{s,cut\text{-}out}$ for sensitivity analysis, all sites*

Appendix C

Control strategies

The results presented in chapter 5 regarding the performance of the control strategies did only include the response when using the high alternative for $H_{s,cut\text{-}out}$ and the shortest reconfiguration time, but all the detailed results for all sites is shown here, in figure C.1, C.2 and C.3.

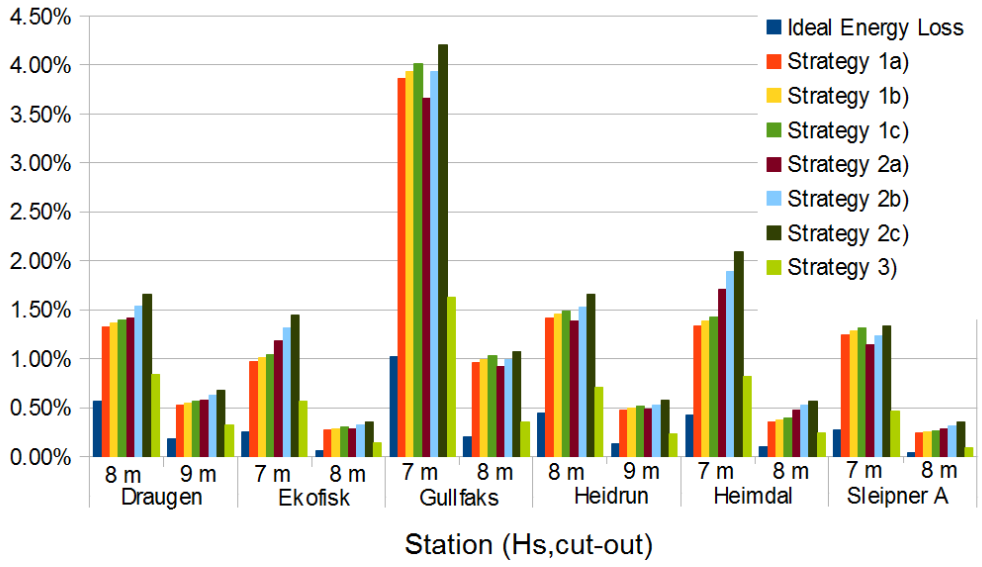

Figure C.1: *Energy loss using different $H_{s,cut\text{-}out}$, strategies and reconfiguration times, all sites*

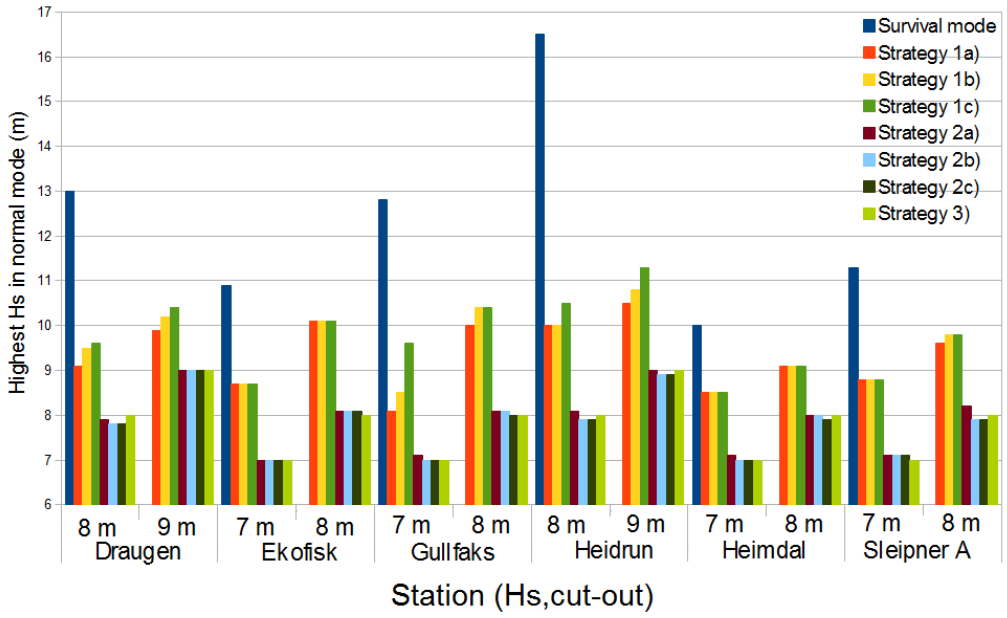

Figure C.2: *Highest wave experienced in normal mode using different $H_{s,cut\text{-}out}$, strategies and reconfiguration times, all sites*

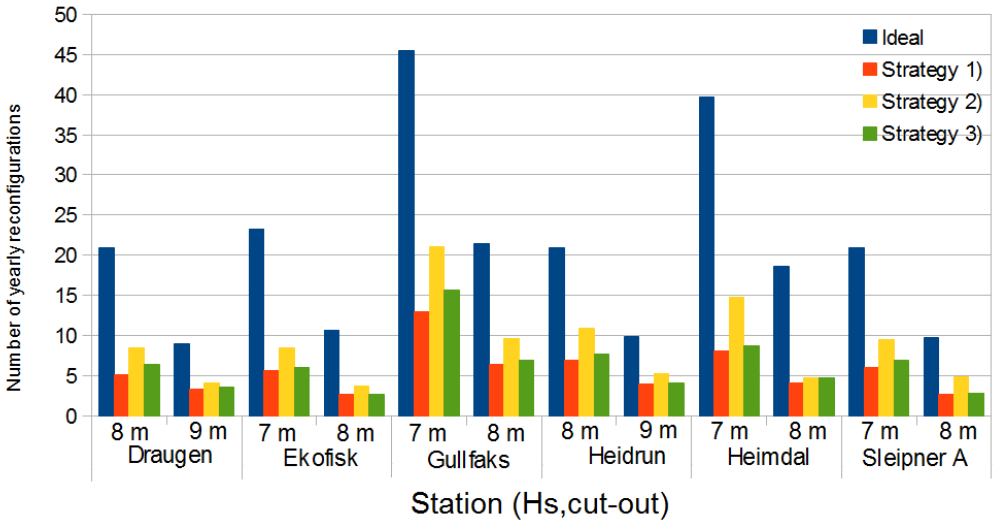

Figure C.3: *Number of yearly reconfigurations using different $H_{s,cut\text{-}out}$, strategies and reconfiguration times, all sites*

Appendix D

Load simulations in 3Dfloat

Two rounds of load simulations were run by Anders Myhr in 3Dfloat. The first round of simulations that was performed in April 2013 investigated the load response of normal and survival mode configuration of mooring lines, known as load case 1 and 2. The TLB was exerted to wave heights from 0 metres up to extreme waves. The value of the extreme wave height was set to $H_s = 15.7$ m, meaning that the turbine was exerted to regular waves with a height of 29 metres assuming that $H_{max} = 1.85 \cdot H_s$.[50]

The turbine was assumed to be placed in a depth of 75 metres, with a mooring line radius of 120 m. The load response of the extreme wave for the top and bottom mooring lines in standard and survival mode is shown in figure D.1 to D.4. Here it can be seen that the load amplitudes increases for the bottom lines and decreases for the top lines when in survival mode.

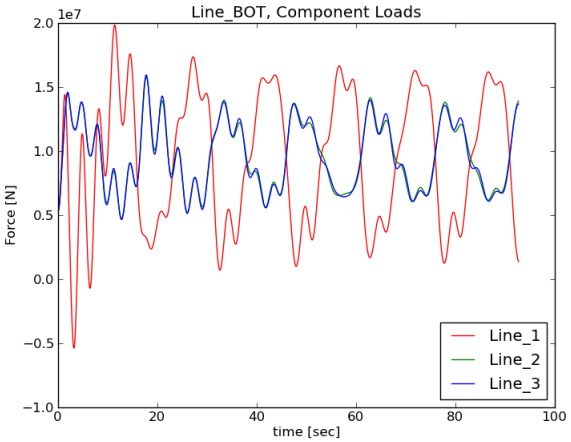

Figure D.1: *Extreme loads on bottom mooring lines in normal configuration [50]*

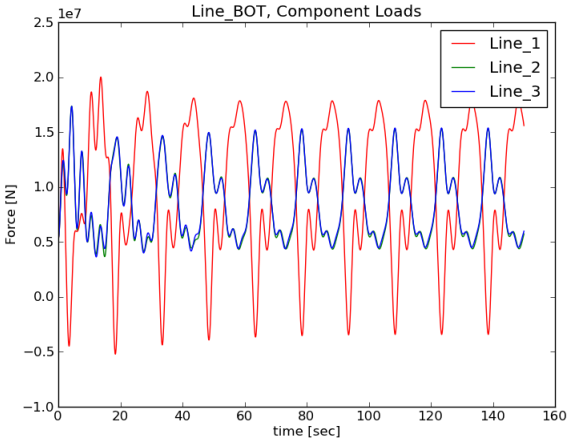

Figure D.2: *Extreme loads on bottom mooring lines in survival mode[50]*

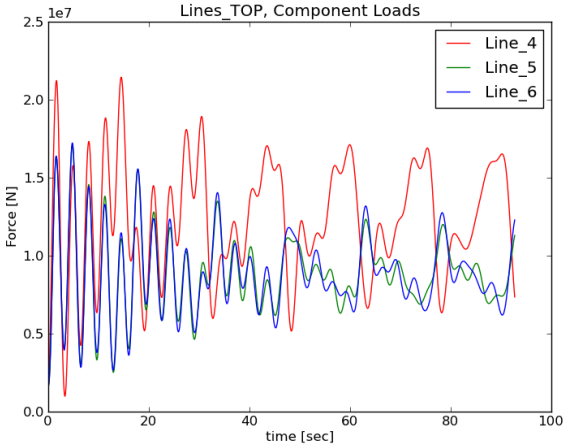

Figure D.3: *Extreme loads on top mooring lines in normal configuration [50]*

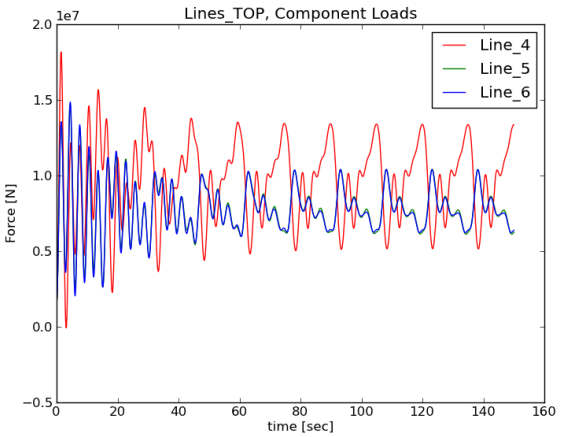

Figure D.4: *Extreme loads on top mooring lines in survival mode [50]*

Some modifications were done when performing last minute simulations in May. First, the mooring line radius was increased to 200 metres. Second, a new configuration of the mooring lines was introduced, Survival05, which placed the upper lines between the standard and survival mode position. This position was found through trial and error. The three different configurations of the TLB were exerted to calm sea and extreme waves and the loads and load amplitudes for the anchors and top and bottom mooring lines are shown in table D.1.

Table D.1: *Load amplitudes for extreme wave and calm sea on mooring lines and anchors for the three different positioning of mooring lines[51]*

	Component	Standard (10^7 N)			Survival05 (10^7 N)			Survival (10^7 N)		
		Min	Max	Amp	Min	Max	Amp	Min	Max	Amp
Extreme	Top lines	0.70	2.50	1.80	1.00	1.90	0.90	1.00	1.50	0.50
	Bottom lines	0.60	2.40	1.80	0.50	2.25	1.75	0.20	2.40	2.20
	Anchors	1.30	4.50	3.20	1.10	4.00	2.90	1.10	3.70	2.60
Calm sea	Top lines	1.50	1.50	0.00	1.40	1.40	0.00	1.20	1.20	0.00
	Bottom lines	1.50	1.50	0.00	1.50	1.50	0.00	1.30	1.30	0.00
	Anchors	1.00	3.00	2.00	1.00	2.70	1.70	1.00	2.40	1.40